

NO-177 699

HIGH-SPEED-PERFORMANCE ANALYSIS MONITORIAL AND OPTIMAL
BOOST CLIMB PERFORMANCE. (U) AIR FORCE WRIGHT
AERONAUTICAL LABS WRIGHT-PATTERSON AFB OH L E MILLER
JAN 87 AFMIL-TR-86-3875 F/8 20/4

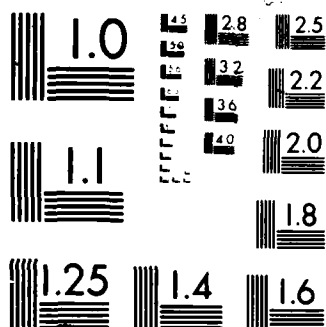
12

UNCLASSIFIED

JAN 87 AFMIL-TR-86-3075

F/8 20/4

■



XERO COPY RESOLUTION TEST CHART

AFWAL-TR-86-3075

HIGH-SPEED-PERFORMANCE ANALYSIS

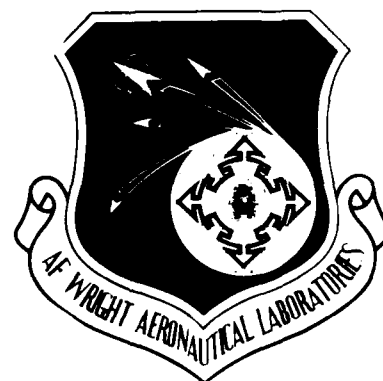
Nominal and Optimal Boost Climb Performance Analysis

L. Earl Miller
High Speed Performance Branch
Aeromechanics Division

January 1987

Final Report for Period July 1985 - March 1986

Approved for Public Release; Distribution Unlimited



DTIC
ELECTE
MAR 17 1987
S D

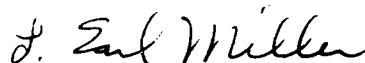
FLIGHT DYNAMICS LABORATORY
AIR FORCE WRIGHT AERONAUTICAL LABORATORIES
AIR FORCE SYSTEMS COMMAND
WRIGHT-PATTERSON AIR FORCE BASE, OHIO 45433-6553

NOTICE

When Government drawings, specifications, or other data are used for any purpose other than in connection with a definitely related Government procurement operation, the United States Government thereby incurs no responsibility nor any obligation whatsoever; and the fact that the government may have formulated, furnished, or in any way supplied the said drawings, specifications, or other data, is not to be regarded by implication or otherwise as in any manner licensing the holder or any other person or corporation, or conveying any rights or permission to manufacture use, or sell any patented invention that may in any way be related thereto.

This report has been reviewed by the Office of Public Affairs (ASD/PA) and is releasable to the National Technical Information Service (NTIS). At NTIS, it will be available to the general public, including foreign nations.

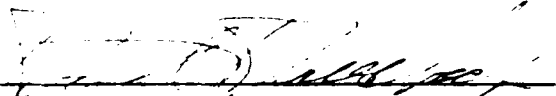
This technical report has been reviewed and is approved for publication.



L. EARL MILLER
Aerospace Engineer
High Speed Aero Performance Branch
Aeromechanics Division
FOR THE COMMANDER



VALENTINE DAHLEM
Chief
High Speed Aero Performance Branch
Aeromechanics Division



DONALD A. DREESBACH, Col, USAF
Chief, Aeromechanics Division

"If your address has changed, if you wish to be removed from our mailing list, or if the addressee is no longer employed by your organization please notify AFWAL/FIMG, W-PAFB, OH 45433- 6553 to help us maintain a current mailing list".

Copies of this report should not be returned unless is required by security considerations, contractual obligations, or notice on a specific document.

UNCLASSIFIED

SECURITY CLASSIFICATION OF THIS PAGE

ADA 177699

REPORT DOCUMENTATION PAGE

1a. REPORT SECURITY CLASSIFICATION UNCLASSIFIED		1b. RESTRICTIVE MARKINGS			
2a. SECURITY CLASSIFICATION AUTHORITY		3. DISTRIBUTION/AVAILABILITY OF REPORT Approved for Public Release; Distribution Unlimited			
2b. DECLASSIFICATION/DOWNGRADING SCHEDULE					
4. PERFORMING ORGANIZATION REPORT NUMBER(S) AFWAL-TR-86-3075		5. MONITORING ORGANIZATION REPORT NUMBER(S)			
6a. NAME OF PERFORMING ORGANIZATION Flight Dynamics Laboratory	6b. OFFICE SYMBOL (If applicable) AFWAL/FIMG	7a. NAME OF MONITORING ORGANIZATION			
6c. ADDRESS (City, State and ZIP Code) Flight Dynamics Laboratory (AFWAL/FIMG) AF Wright Aeronautical Laboratories (AFSC) Wright-Patterson AFB, OH 45433-6553		7b. ADDRESS (City, State and ZIP Code)			
8a. NAME OF FUNDING/SPONSORING ORGANIZATION	8b. OFFICE SYMBOL (If applicable)	9. PROCUREMENT INSTRUMENT IDENTIFICATION NUMBER			
8c. ADDRESS (City, State and ZIP Code)		10. SOURCE OF FUNDING NOS			
		PROGRAM ELEMENT NO.	PROJECT NO	TASK NO	WORK UNIT NO
11. TITLE (Include Security Classification) HIGH-SPEED PERFORMANCE ANALYSIS - Nominal and Optimal (over)		62201F	2404	07	66
12. PERSONAL AUTHOR(S) L. Earl Miller					
13a. TYPE OF REPORT Final	13b. TIME COVERED FROM Jul 85 TO Mar 86	14. DATE OF REPORT (Yr., Mo., Day) 1987 January		15. PAGE COUNT 96	
16. SUPPLEMENTARY NOTATION					
17. COSATI CODES			18. SUBJECT TERMS (Continue on reverse if necessary and identify by block number)		
FIELD	GROUP	SUB. GR.			
19. ABSTRACT (Continue on reverse if necessary and identify by block number)					
<p>Nominal and optimal boost climb trajectories were developed for an air-launched vehicle. The agreement between approximate nominal and exact numerical solutions was quite good. Three payoffs were addressed for the optimal trajectories; maximum speeds at burnout or apogee, minimum fuel to apogee, and minimum time to apogee. The last two are equivalent since the fuel-burning rate was constant. Thrust vectoring was considered for one problem, but the difference relative to zero thrust vectoring was negligible. The remaining problems only considered zero thrust vectoring. In general, the optimal angle-of-attack decreased with increasing time. The change was greater for the minimum time solution. For this case, a fast pitch-up occurred initially and then the angle-of-attack rapidly decreased to the angle-of-attack for $-C_{LMAX}$. The gave the fastest pitch over to apogee. The minimum time solution may reach apogee before burn-out. This never occurs for the maximum speed case; the terminal condition is reached at or after burn-out.</p>					
20. DISTRIBUTION/AVAILABILITY OF ABSTRACT UNCLASSIFIED/UNLIMITED <input checked="" type="checkbox"/> SAME AS RPT. <input type="checkbox"/> DTIC USERS <input type="checkbox"/>			21. ABSTRACT SECURITY CLASSIFICATION UNCLASSIFIED		
22a. NAME OF RESPONSIBLE INDIVIDUAL L. Earl Miller		22b. TELEPHONE NUMBER (Include Area Code) (513) 255-2021		22c. OFFICE SYMBOL AFWAL/FIMG	

DD FORM 1473, 83 APR

EDITION OF 1 JAN 73 IS OBSOLETE

UNCLASSIFIED
SECURITY CLASSIFICATION OF THIS PAGE

UNCLASSIFIED

SECURITY CLASSIFICATION OF THIS PAGE

Block 11 (Continued)

Boost Climb Performance Analysis

UNCLASSIFIED

SECURITY CLASSIFICATION OF THIS PAGE

FOREWORD

This report was prepared by Dr Earl Miller of the High Speed Aero Performance Branch, Aeromechanics Division, Flight Dynamics Laboratories, Wright-Patterson Air Force Base, Ohio. This research was accomplished under job order number 24040766, "High Speed Performance Analysis." This effort was conducted during the period from July 1985 to March 1986.



Accession For	
NTIS CRA&I	<input checked="" type="checkbox"/>
DTIC TAB	<input type="checkbox"/>
Unannounced	<input type="checkbox"/>
Justification	
By	
Distribution /	
Availability Codes	
Dist	Availability for Special
A-1	

TABLE OF CONTENTS

SECTION	TITLE	PAGE
I	INTRODUCTION	1
II	ASSUMPTIONS	2
	Spherical Symmetry	2
	Exponential Atmosphere	2
	Aerodynamic Data	4
	Propulsion Characteristics	9
	Equations of Motion	9
III	NOMINAL BOOST AND CLIMB PERFORMANCE	11
	Maximum Lift, Power-On	14
	Constant Flight Path, Power-On	17
	Zero Angle-of-Attack, Power-On	18
	Zero Angle-of-Attack, Power-Off	20
	Complete Trajectories	21
IV	OPTIMAL BOOST CLIMB PERFORMANCE	22
	Aerodynamic Relations	23
	Optimal Control Problem	24
	Optimal Trajectory Solutions	28
V	CONCLUSIONS	31
	REFERENCES	33
	APPENDIX	35
	CORRELATION BETWEEN EXPERIMENTAL AND THEORETICAL AERODYNAMIC DATA	

LIST OF FIGURES

FIGURE	TITLE	PAGE
1	Optimum Angle of Attack	49
2	C_{D_o}/K	50
3	Lift to Drag Ratio	51
4	$C_L(\alpha), \frac{1}{3}C_{D_\alpha}(\alpha)$	52
5	$C_D(\alpha)$	53
6	$C_{L_\alpha}(\alpha), \frac{1}{3}C_{D_{\alpha\alpha}}(\alpha)$	54
7	$C_{L_{\alpha\alpha}}(\alpha)$	55
8	$P_R(\alpha^*)$	56
9	$\delta_v^*(\alpha^*)$	57
10	$F(\delta_v^*)$	58
11	$G(\alpha^*)$	59
12	$F_{\delta_v\delta_v}(\delta_v^*)$	60
13	$G_{\alpha\alpha}(\alpha^*)$	61
14	$P_R(\alpha^*), \delta_v = 0$	62
15	$G(\alpha^*), \delta_v = 0$	63
16	$G_{\alpha\alpha}(\alpha^*), \delta_v = 0$	64

LIST OF FIGURES (cont'd)

FIGURE	TITLE	PAGE
17	Optimal Speed, Problem 1	65
18	Flight Path Angle, Problem 1	66
19	Altitude, Problem 1	67
20	P_R , Problem 1	68
21	P_S , Problem 1	69
22	α^* , Problem 1	70
23	δ_V^* , Problem 1	71
24	Speed for Problems 2, 3, 4. $\gamma(t_f) = 0, \delta_V = 0$	72
25	Flight Path Angle for Problems 2, 3, 4. $\gamma(t_f) = 0, \delta_V = 0$	73
26	Altitude for Problems, 2, 3, 4. $\gamma(t_f) = 0, \delta_V = 0$	74
27	Optimal Angle of Attack for Problems 2, 3, 4. $\gamma(t_f) = 0, \delta_V = 0$	75
A.1	Configurations	76
A.2	AMI Aerodynamic Characteristics	77
A.3	Lift to Drag Ratio for Optimum Configuration	78

LIST OF FIGURES (cont'd)

FIGURE	TITLE	PAGE
A.4	X24C Aerodynamic Characteristics	79
A.5	DYNASOAR Aerodynamic Characteristics	80
A.6	SHUTTLE Aerodynamic Characteristics	81
A.7	ASSET Aerodynamic Characteristics	82
A.8	SORTIE Aerodynamic Characteristics	83

LIST OF TABLES

TABLE	TITLE	PAGE
1	ATMOSPHERIC PARAMETERS	38
2	EXPONENTIAL DENSITY ERRORS	38
3	AERODYNAMIC PARAMETERS	39
4	EXACT AND APPROXIMATE AERODYNAMIC PARAMETERS	39
5	SAMPLE BOOSTER PROPULSION CHARACTERISTICS	40
6	INITIAL ROTATION RESULTS	41
7	CONSTANT FLIGHT PATH, POWER-ON COMPARISONS	42
8	ZERO ANGLE-OF-ATTACK, POWER-ON COMPARISONS	43
9	ZERO ANGLE-OF-ATTACK, POWER-OFF COMPARISONS	44
10	COMPLETE TRAJECTORY COMPARISONS	45
11	OPTIMAL CONTROL PROBLEMS	46
12	SELECTED OPTIMAL CONTROL PROBLEMS	47
13	PROBLEM 1 RESULTS	47
14	OPTIMAL TRAJECTORY RESULTS	48
A	AERODYNAMIC PARAMETERS	48

LIST OF SYMBOLS

A	density parameter, area
B	density parameter
C	drag parameter
C_D	drag coefficient
C_{D_0}	zero lift drag coefficient
C_L	lift coefficient
C_P	pressure coefficient
D	aerodynamic drag
d	drag to weight ratio
E	lift to drag ratio
f_T, f_N	nondimensional force functions
F, G	control functions
F_T, F_N	external forces
g	acceleration of gravity
h	altitude
H	Hamiltonian function
\bar{i}	unit vector along velocity vector

LIST OF SYMBOLS (cont'd)

I_{SP}	specific impulse
I_{TOTAL}	total impulse
\bar{k}	unit vector normal to velocity vector
K	Newtonian pressure coefficient
L	aerodynamic lift
m	mass
M	mean molecular weight of air
n	lift to weight ratio
$n(0)$	initial lift to weight ratio
\bar{n}	unit normal outward vector to surface
P_u, P_v, P_G	costate variables
q	dynamic pressure
r	radius from center of earth
R	radius of earth
R^*	universal gas constant
S	reference aerodynamic area
t	time

LIST OF SYMBOLS (cont'd)

t_B	burn time
t_{BO}	burn out time
t_o	initial time
T	temperature, thrust
u	nondimensional speed
V	speed
ΔV	incremental speed
W	weight
W_{PROP}	propellant weight

GREEK CHARACTERS

α	angle of attack
α_o	reference angle of attack
β	nondimensional time
β_o	nondimensional initial time
β_f	nondimensional final time
γ	flight path angle
γ_c	constant flight path angle

LIST OF SYMBOLS (cont'd)

δ	$\alpha + \delta_v$, angle between outward normal and velocity
δ_v	thrust vector angle
θ	longitude
λ_i	performance parameters ($i = 1, \dots, 5$)
ρ	density
σ	density ratio, bank angle
τ	$T/W(0)$
ϕ	latitude
ψ	heading
ω	earth rotational rate, nondimensional weight
μ	lift function

SUBSCRIPT

$()_R$	reference condition
$()_{ACT}$	actual value
$()_{THEOR}$	theoretical value

LIST OF SYMBOLS (cont'd)

SUPERSCRIPTS

- * optimal value
- ($\dot{}$) time rate of change of ()
- (') derivative of () with respect to β

SECTION 1

INTRODUCTION

There exists in the literature several papers on the flight mechanics of reentry vehicles. Unfortunately, there is little in the literature that focuses on the ascent performance of a booster configuration from launch to apogee. Consequently, there is a need for both approximate analytical and exact numerical trajectory solutions. The former could be used for preliminary design purposes. The latter could be used for performance trade-offs of finalized configurations.

This investigation has two objectives. The first is to develop approximate analytical trajectory solutions. The second is to determine optimal trajectories for a specified criterion. Numerical results will be for a specific configuration. The approximate solutions are segments for an ascent trajectory that can be patched together to yield a complete ascent trajectory. The segments are maximum lift with power-on, constant flight path with power-on, and zero angle-of-attack with both power-on and power-off. For the optimal trajectories, the payoffs are maximum speed at burnout or apogee and minimum fuel or time to reach apogee.

In Section II, the assumptions employed in the investigation are presented. Sections III and IV contain the approximate and optimal trajectory results.

SECTION II

ASSUMPTIONS

Spherical Symmetry

The modeling of the atmospheric density and the acceleration of gravity can be greatly simplified if it can be assumed that: 1) the density is a function of only the altitude and 2) the acceleration of gravity is a function of only the radial distance from the center of the planet. The earth's surface is an oblate spheroid of eccentricity 0.00335. The ratio of the radius at the poles to that at the Equator is 0.99665. The difference in the surface radius at the equator and either pole is approximately seventy thousand feet. The ratio of the acceleration of gravity at the poles to that at the equator is approximately 1.0018. For the purpose of this effort, it suffices to treat the earth as spherical

The acceleration varies inversely proportional as the square of the radius from the center of earth. The nominal thickness of the earth's atmosphere is of the order of 275,000 feet. The ratio of the acceleration of gravity at the outer edge of the atmosphere to that at the earth's surface is approximately 0.972. In this study the acceleration of gravity will be assumed to be constant. The sea level value of 32.174 feet/second/second will be used.

Exponential Atmosphere

The relationship for the rate of change of density with respect to altitude can be approximated by

$$\frac{dp}{dh} = B\rho \quad (1)$$

where

$$B = - \frac{gM}{R^*T} = - \frac{1}{T} \frac{dT}{dh} \quad (2)$$

The density relation is exact across layers where the temperature is constant. In layers where the temperature is linear with respect to altitude, Equation (1) is approximate. If an approximate value is used across the latter layer, then Equation (1) takes on the following form for all layers.

$$\rho = \rho_R e^{B(h - h_R)} \quad (3)$$

Let

$$y = \ln \rho, \quad A = \ln \left(\rho_R e^{-Bh_R} \right) \quad (4)$$

Then Equation (3) can be rewritten as

$$y = A + Bh \quad (5)$$

Approximation for A and B can be determined by doing regression analysis on Equation (5). Using the 1962 U.S. Standard Atmosphere as the basis gives the results in Table 1.

The accuracy of these approximations are presented in Table 2 where the error is defined as

$$\% \text{ ERROR} = \frac{\sigma_{\text{ACT}} - \sigma_{\text{THEOR}}}{\sigma_{\text{ACT}}} \times 100$$

and σ_{ACT} is the 1962 density ratio and σ_{THEOR} is the approximate value. The assumed form for the density ratio for the subsequent performance analysis is

$$\sigma = e^{Bh + A} \quad (6)$$

Aerodynamic Data

For high speed trajectory analysis it will be assumed that the aerodynamic coefficients can be predicted by Newtonian theory. This theory is based upon the assumption that the pressure at any point on the windward side of the vehicle can be predicted by

$$C_p = K(\bar{n} \cdot \bar{i})^2 \quad (7)$$

Let the scalar product be defined by $\sin\delta$, then

$$C_p = k \sin^2 \delta \quad (8)$$

The drag and lift components due to the pressure force are evaluated from

$$\frac{L}{q} = \int \int C_p (\bar{k} \cdot \bar{n}) dA \quad (9)$$

$$\frac{D}{q} = \int \int C_p (\bar{i} \cdot \bar{n}) dA \quad (10)$$

Since

$$\bar{k} \cdot \bar{n} = \cos\delta \quad (11)$$

Equations (9) and (10) become

$$\frac{L}{q} = K \int \int \sin^2 \delta \cos \delta dA \quad (12)$$

$$\frac{D}{q} = K \int \int \sin^3 \delta dA \quad (13)$$

If the angle δ is constant everywhere over the vehicle then the drag and lift coefficients become

$$C_L = \frac{L}{qA} = K \sin^2 \delta \cos \delta \quad (14)$$

$$C_D = \frac{D}{qA} = K \sin^3 \delta \quad (15)$$

An additional component should be added to the drag coefficient to account for bluntness and viscous effects, thus

$$C_D = K \sin^3 \delta + C_{D_0} \quad (16)$$

The increment C_{D_0} is a strong function of nose bluntness and generally is also altitude dependent.

The approximation is going from Equations (12) and (13) to Equations (14) and (15) is presented in the appendix where

$$\delta = \alpha + \alpha_0 \quad (17)$$

Seven different configurations were examined. The correlation shows that Equations (14) and (16) are adequate for the purpose of this investigation.

Previous studies have shown that for reentry trajectory analysis, the lift-to-drag ratio is an important parameter. For ascent performance, the lift coefficient versus angle-of-attack is an important function for high thrust to weight rocket engines. Consider the aerodynamic ratio E defined by

$$E = \frac{L}{D} = \frac{K \sin^2 \delta \cos \delta}{K \sin^3 \delta + C_{D_0}} = \frac{\sin^2 \delta \cos \delta}{\sin^3 \delta + C} \quad (18)$$

where

$$C = \frac{C_{D_0}}{K} \quad (19)$$

The maximum value of L/D , E^* , is obtained by optimizing with respect to δ . Differentiating Equation (18) with respect to δ and setting the resulting expression equal to zero gives the necessary condition for E^*

$$\sin^3 \delta^* + 3C \sin^2 \delta^* - 2C = 0 \quad (20)$$

This equation can be easily solved for δ^* as a function of C . In general, however, we are interested in determining the parameters δ^* and C as a function of E^* . Solving Equation (18) for C gives

$$C = \frac{1}{E^*} \cdot \sin^2 \delta^* \cos \delta^* - \sin^3 \delta^* \quad (21)$$

Substituting Equation (21) for C into Equation (20) gives a relation between E^* and δ^*

$$E^* = \frac{2 - 3\sin^2 \delta^*}{3\sin \delta^* \cos \delta^*} \quad (22)$$

Using double angle formulas, this reduces to

$$E^* = \frac{\frac{1}{3} + \cos^2 \delta^*}{\sin^2 \delta^*} \quad (23)$$

This is easily solved for δ^* as a function of E^*

$$\cos^2 \delta^* = \frac{-\frac{2}{3} + 2E^* \left(E^{*2} + \frac{8}{9} \right)^{1/2}}{2(E^{*2} + 1)} \quad (24)$$

Given E^* , δ^* is determined from Equation (24) and C is obtained from Equation (21). These parameters and the ratio of C_D at δ^* to C_{D_0} are presented in Table 3.

For a parabolic polar, $C_D(\delta^*)/C_{D_0}$ is 2.

The maximum value of the lift coefficient is obtained from optimization of Equation (14) with respect to δ . The necessary condition is

$$2\sin\delta\cos^2\delta - \sin^3\delta = 0 \quad (25)$$

The solution for δ is

$$\delta = \sin^{-1}(2/3)^{1/2} = 54.74^\circ \quad (26)$$

The value of maximum C_L is

$$C_{L_{MAX}} = 0.3849K \quad (27)$$

In Figures 1 through 3, the aerodynamic parameters are presented. In Figures 1 and 3, δ equals α .

The drag coefficient can be written in polar form by eliminating δ from the C_L and C_D relations. Expanding Equation (14) gives a cubic equation in $\sin^2\delta$. The solution of this cubic equation is

$$\sin^2\delta = \frac{1}{3} \cdot (1 - \cos\mu + \sqrt{3}\sin\mu) \quad (28)$$

where

$$\mu = \frac{1}{3} \cdot \cos^{-1} \left[1 - \frac{27}{2} \cdot \left(\frac{C_L}{K} \right)^2 \right] \quad (29)$$

Substituting for $\sin\delta$ in Equation (16) gives

$$C_D = C_{D_0} + K \left[\frac{1}{3} (1 - \cos \mu + \sqrt{3} \sin \mu) \right]^{3/2} \quad (30)$$

For small values of C_L/K , the parameters become approximately

$$\sin \delta = \sqrt{\frac{C_L}{K}} \quad (31)$$

$$C_D = C_{D_0} + \frac{C_L^{3/2}}{K^{1/2}} \quad (32)$$

The optimal value for C_L^* is

$$C_L^* = (2K^{1/2} C_{D_0})^{2/3} \quad (33)$$

The optimal value for C_D^* is

$$C_D^* = 3C_{D_0} \quad (34)$$

The maximum value of E is

$$E^* = \frac{1}{3} \left(\frac{4K}{C_{D_0}} \right)^{1/3} \quad (35)$$

In Table 4, exact aerodynamic parameters from Equations (14) and (16) and approximate values from previous relations are presented. It can be seen that a polar of the form in Equation (32) gives fairly good agreement for E^* when E^* is greater than 1.5. If the trajectory requires very accurate data for C_L and C_D , then the approximate relations should not be used. Accurate data should be used with accurate interpolation techniques employed.

Propulsion Characteristics

Rocket propulsion characteristics will be used for the performance analysis. The mass burning rate is determined from

$$\dot{W} = - \frac{W_{PROP}}{t_B} \quad (36)$$

The burn time, t_B , is determined from

$$t_B = \frac{I_{TOTAL}}{T} \quad (37)$$

where I_{TOTAL} is the total impulse and has units (force)x(time). Table 5 presents propulsion characteristics for several boosters. The speed change, ΔV , corresponds to the gravity free solution in a vacuum.

Equations of Motion

From Reference 2, the equations of motion for the trajectory analysis are

$$\frac{dv}{dt} = \frac{1}{m} \cdot F_T - g \sin \gamma + \omega^2 r \cos \phi (\sin \gamma \cos \phi - \cos \gamma \sin \psi \sin \phi) \quad (38)$$

$$\begin{aligned} V \frac{d\gamma}{dt} = & \frac{1}{m} \cdot F_N \cos \sigma - g \cos \gamma + \frac{V^2}{r} \cdot \cos \gamma + 2\omega V \cos \psi \cos \phi \\ & + \omega^2 r \cos \phi (\cos \gamma \cos \phi + \sin \gamma \sin \psi \sin \phi) \end{aligned} \quad (39)$$

$$\begin{aligned} V \frac{d\psi}{dt} = & \frac{1}{m} \cdot \frac{F_N \sin \sigma}{\cos \gamma} - \frac{V^2}{r} \cdot \cos \gamma \cos \psi \tan \phi + 2\omega V (\tan \gamma \sin \psi \cos \phi) \\ & - \sin \phi) - \frac{\omega^2 r}{\cos \gamma} \cdot \cos \psi \sin \phi \cos \phi \end{aligned} \quad (39)$$

$$\frac{dr}{dt} = V \sin \gamma \quad (41)$$

$$\frac{d\theta}{dt} = \frac{V \cos \gamma \cos \psi}{r \cos \phi} \quad (42)$$

$$\frac{d\phi}{dt} = \frac{V \cos \gamma \sin \psi}{r} \quad (43)$$

$$F_T = T \cos(\alpha + \delta_v) - D \quad (44)$$

$$F_N = T \sin(\alpha + \delta_v) + L \quad (45)$$

Some of the terms in Equations (38) through (40) can be dropped. The transport acceleration, $\omega^2 r$, is less than 0.4 percent of the acceleration of gravity. The Coriolis acceleration, $2\omega V$, is approximately eleven percent of the acceleration of gravity and therefore is important for long range high speed flight. For low speed, short range trajectory, this term can be neglected. For example, a boost and coast to apogee trajectory can neglect the earth's rotation. Also for boost and coast to apogee problems, the term V^2/r in Equations (39) and (40) can be neglected since these types of trajectories are over short ranges. Thus, the earth can be treated as flat.

In the next section, we turn our attention to the boost and coast to apogee problems.

SECTION III

NOMINAL BOOST AND CLIMB PERFORMANCE

Both ground launches and air launches are important problems. The primary difference between them is the boundary conditions. Ground launch initial conditions are zero speed and ninety degree launch angles. Air launches correspond to the speed of the launch platform and zero flight path angle. This effort has concentrated on air launches only.

A typical trajectory consists of the separation from the carrier, propulsion ignition, pitch up to a specified attitude, and then an acceleration to burnout. This may be followed by the separation of the booster and then a second boost to a second burnout. After the boost phase or phases, the vehicle coasts and decelerates to apogee. An impulse may follow to give the desired orbital speed.

Five different boost and climb segments are of interest. They are as follows:

- a. maximum lift, power-on
- b. constant flight path, power-on
- c. zero angle-of-attack, power-on
- d. zero angle-of-attack, power-off
- e. optimum boost climb

The last problem is addressed in Section IV. This problem is difficult and merits attention in a section by itself. The difficulty is determining the optimal controls. The first four

make up a typical sequence from launch to apogee. Each of the first four problems is solved in the following subsections.

Flight is in the equational plane and the earth's rotation is neglected. The equation for the rate of change of r , \dot{r} , is replaced with the time rate of change of the density. The result is

$$\dot{\sigma} = B\sigma V \sin \gamma \quad (46)$$

where B is defined in Equation (6). The remaining differential equations are

$$\dot{W} = - \frac{T}{I_{SP}} \quad (47)$$

$$\dot{V} = \frac{1}{m} \cdot F_T - g \sin \gamma \quad (48)$$

$$\dot{\gamma} = \frac{1}{mV} \cdot F_N - \frac{g}{V} \cdot \cos \gamma \quad (49)$$

$$\dot{\theta} = \frac{V}{r} \cdot \cos \gamma \quad (50)$$

where

$$F_T = T \cos(\alpha + \delta_v) - D \quad (51)$$

$$F_N = T \sin(\alpha + \delta_v) + L \quad (52)$$

Nondimensional transformation are introduced in order to normalize the variables to the order of one. Let

$$u = V/V(0), \quad \omega = W/W(0), \quad \beta = t/t_R \quad (53)$$

We are free to select the reference time, t_R . The differential equations become

$$\sigma' = \lambda_1 \sigma u \sin \gamma \quad (54)$$

$$\omega' = -\lambda_2 \quad (55)$$

$$u' = \lambda_3 \left(\frac{\tau}{\omega} \cos \delta - d - \sin \gamma \right) \quad (56)$$

$$\gamma' = \frac{\lambda_3}{u} \left(\frac{\tau}{\omega} \sin \delta + n - \cos \gamma \right) \quad (57)$$

$$\theta' = \lambda_4 u \cos \gamma \quad (58)$$

where

$$\lambda_1 = t_R^{BV(0)} \quad (59)$$

$$\lambda_2 = \frac{t_R T}{W(0) I_{SP}} = \frac{W_{PROP}}{W(0)} \quad (60)$$

$$\lambda_3 = \frac{g t_R}{V(0)} \quad (61)$$

$$\lambda_4 = \frac{V(0) t_R}{R} \quad (62)$$

$$\delta = \alpha + \delta_V \quad (63)$$

$$d = \frac{D}{W}, \quad n = \frac{L}{W}, \quad \tau = \frac{T}{W(0)} \quad (64)$$

In Equation (50), r has been approximated by R . In Equation (62), the parameter λ_4 is very small. Thus the change in the downrange is small. In Equations (54) through (58), differentiation is with respect to the nondimensional time β .

The approach is to develop approximate closed form solutions for the different trajectory segments. These approximate solutions are compared with the exact solutions obtained by numerical integration of the differential equations of motion.

This comparison offers some evidence as to the fidelity of the approximate solutions. As expected, some accuracy is lost through introducing assumptions that make it possible to analytically integrate the differential equations. But, one advantage is that an approximate solution can be easily obtained through substitution of specific values for the parameters. We turn our attention to the first problem. The booster characteristics correspond to configuration 17 in Table 5.

Maximum Lift, Power-On

This segment corresponds to the initial rotation after launch. The initial conditions are the launch conditions. The terminal conditions are free. Integrating Equation (55) gives:

$$\omega = 1 - \lambda_2 \beta \quad (65)$$

Assume that the flight path angle is small and the angle-of-attack is constant. Also, assume that the change in the drag coefficient is negligible, which is a questionable assumption, and the change in the density is negligible, which is reasonable. Then the drag ratio in Equation (64) is approximately

$$d = \frac{u^2}{\omega} \cdot d(0) \quad (66)$$

Equation (56) is approximately

$$u' = \frac{\lambda_3}{\omega} \cdot [\tau \cos \delta - u^2 d(0)] \quad (67)$$

Combining with Equation (55) and integrating gives

$$u = \lambda_5 \frac{\frac{\lambda_5 + 1}{\lambda_5 - 1} \omega^{-\lambda_6} - 1}{\frac{\lambda_5 + 1}{\lambda_5 - 1} \omega^{-\lambda_6} + 1} \quad (68)$$

where

$$\lambda_5 = \sqrt{\frac{\tau \cos \delta}{d(0)}} \quad , \quad \lambda_6 = 2 \frac{\lambda_3}{\lambda_2} \cdot \sqrt{\tau d(0) \cos \delta} \quad (69)$$

In a manner like that for d , n is approximately

$$n = n(0) \cdot \frac{u^2}{\omega} \quad (70)$$

At high angles-of-attack, the right side of Equation (57) is approximately n , since

$$n \gg \frac{\tau}{\omega} \cdot \sin \delta - \cos \gamma \quad (71)$$

Combining approximate forms for Equations (56) and (57) gives

$$\frac{d\gamma}{du} = \frac{n(0)u}{\tau \cos \delta - d(0)u^2} \quad (72)$$

Integrating gives

$$\gamma = \gamma(0) - \frac{1}{2} E(0) \ln \frac{f_T}{f_T(0)} \quad (73)$$

where

$$E(0) = \frac{n(0)}{d(0)} = \frac{L(0)}{D(0)} = \frac{C_L(0)}{C_D(0)}, \quad f_T = \tau \cos \delta - d(0)u^2 \quad (74)$$

Combining Equations (54) and (56) gives approximately

$$\frac{d\sigma}{du} = \frac{\lambda_1 \sigma u \gamma}{\frac{\lambda_3}{\omega} [\tau \cos \delta - d(0)u^2]} \quad (75)$$

If the change in the weight is neglected, i.e., assume $\omega = 1$, then Equation (75) can be integrated

$$\begin{aligned} \ln \frac{\sigma}{\sigma(0)} = & - \frac{1}{2d(0)} \cdot \frac{\lambda_1}{\lambda_3} \cdot \left[\gamma(0) + \frac{1}{2} E(0) \ln f_t(0) \right] \ln \frac{f_T}{f_T(0)} \\ & + \frac{E(0)}{8d(0)} \cdot \frac{\lambda_1}{\lambda_3} \cdot \left\{ \left[\ln f_T \right]^2 - \left[\ln f_T(0) \right]^2 \right\} \end{aligned} \quad (76)$$

Combining Equations (58) and (56) gives approximately

$$\frac{d\theta}{du} = \frac{\lambda_4 u}{\frac{\lambda_3}{\omega} [\tau \cos \delta - d(0)u^2]} \quad (77)$$

Assuming $\omega = 1$ permits integration

$$\theta = \theta(0) - \frac{1}{2d(0)} \cdot \frac{\lambda_4}{\lambda_3} \cdot \ln \frac{f_T}{f_T(0)} \quad (78)$$

In Table 6, the comparison between the exact and approximate solutions is presented for the first ten seconds. The flight path reached approximately thirty degrees. In light of the fact that the exact solution included acceleration through the transonic region, the agreement is quite good. The density used in the results correspond to tabular values rather than Equation (6). Equation (6) gives a lower density, approximately 5.5 percent. Using this approximate value in the equation for $d(0)$ results in little difference for the speed, altitude, and downrange. But the flight path angle is lower by approximately

5.5 percent. The drag and lift coefficients are the initial values.

Constant Flight Path, Power-On

This is a path that could be followed once the initial rotation is completed. The objective for this type of trajectory is to establish an attitude or flight path angle that will result in attaining specified apogee conditions. Generally, the angle-of-attack is small since high longitudinal accelerations are desired for constant flight path angles. Equation (57) gives

$$\tau \sin \delta + w n = w \cos \gamma(0) \quad (79)$$

The right side decreases with increasing time; therefore, the angle-of-attack must decrease as the speed increases. The initial conditions are those at the beginning of the segment which are the final conditions at the end of the previous segment, e.g., the initial rotation.

It is assumed that the change in the drag in Equation (56) is negligible. Combining Equations (55) and (56) and integrating gives

$$u = 1 - \frac{\lambda_3}{\lambda_2} \cdot [\tau \cos \delta - d(0)] \ln w + \frac{\lambda_3}{\lambda_2} \cdot (w - 1) \sin \gamma(0) \quad (80)$$

Combining Equations (54) and (55), substituting Equation (80), and then integrating gives

$$\ln \frac{\sigma}{\sigma(0)} = - \frac{\lambda_1}{\lambda_2} \cdot \sin \gamma(0) \left\{ (\omega - 1) - \frac{\lambda_3}{\lambda_2} \cdot [\tau \cos \delta - d(0)] \right. \\ \left. \cdot [\omega \ln \omega - (\omega - 1)] + \frac{1}{2} \cdot \frac{\lambda_3}{\lambda_2} \cdot (\omega - 1)^2 \sin \gamma(0) \right\} \quad (81)$$

Combining Equation s(58) and (54) and integrating gives

$$\theta = \theta(0) + \frac{\lambda_4}{\lambda_1} \cdot \cot \gamma(0) \cdot \ln \frac{\sigma}{\sigma(0)} \quad (82)$$

The exact and approximate solutions are presented in Table 7. The agreement is surprisingly good in light of the assumption made about the drag.

Zero Angle-of-Attack, Power-On

Along this path, the lift is zero and the drag coefficient is minimum since C_D equals C_{D_0} . This corresponds to maximum acceleration, at least on a point performance basis. Over the total segment, however, the integration of the drag may be larger relative to positive angles-of-attack. This is attributed to the fact that a zero angle-of-attack trajectory is lower in the atmosphere; thus, the dynamic pressure may be higher.

It will be assumed that the change in C_{D_0} is negligible and the flight path angle is small. The flight path angle decreases as the vehicle accelerates. It is assumed that the change in the drag is negligible. The speed increases, but the density ratio decreases. Equation (56) reduces to

$$u' = \frac{\lambda_3}{\omega} \cdot [\tau - d(0)] \quad (83)$$

Combining with Equation (55) and integrating gives

$$u = 1 - \frac{\lambda_3}{\lambda_2} \cdot [\tau - d(0)] \ln \omega \quad (84)$$

The inverse of this is required in order to integrate γ'

$$\omega = e^{C(1-u)} \quad (85)$$

where

$$C = \frac{\lambda_2}{\lambda_3 [\tau - d(0)]} \quad (86)$$

Combining the approximate differential forms for u and γ , substituting for ω , and then integrating gives

$$\gamma = \gamma(0) - \frac{\lambda_3}{\lambda_2} \cdot C e^C \left[\ln u + \sum_{i=1}^{\infty} \frac{(-Cu)^i - (-C)^i}{i \cdot i!} \right] \quad (87)$$

Combining Equations (54) and (56), substituting Equation (85) and integrating gives

$$\frac{\lambda_3 f_T}{\lambda_1} \cdot \ln \frac{\sigma}{\sigma(0)} = - \frac{e^C}{C^2} \cdot \left[e^{-Cu} (Cu + 1) \gamma - e^{-C} (C + 1) \gamma(0) \right] \quad (88)$$

$$- \frac{e^{2C}}{f_T C^2} \cdot \left[- \frac{1}{2} \cdot (e^{-2Cu} - e^{-2e}) + \ln u + \sum_{i=1}^{\infty} \frac{(-1)^i (2C)^i}{i \cdot i!} (u^i - 1) \right]$$

where

$$f_T = \tau - d(0) \quad (89)$$

Combining the approximate differential equations for θ and u and integrating gives

$$\theta = \theta(0) + \frac{\lambda_4 e^C}{\lambda_3 f_T C^2} \cdot \left[(C + 1)e^{-C} - (Cu + 1)e^{-Cu} \right] \quad (90)$$

The solution for the nondimensional weight is

$$\omega = 1 - \lambda_2 \beta \quad (91)$$

The exact and approximate solutions are presented in Table 8. The agreement is quite good.

Zero Angle-of-Attack, Power-Off

This segment is the path after burnout up to apogee. The objective is to reach apogee with minimum loss of energy. This corresponds to minimum drag which is zero angle-of-attack on a point performance basis. Assume that the aerodynamic forces are negligible relative to the gravity. Equations (56) and (57) can be combined to give

$$\frac{du}{d\gamma} = u \tan \gamma \quad (92)$$

This is easily integrated to give

$$u = \frac{\cos \gamma(0)}{\cos \gamma} \quad (93)$$

Substituting for u in Equation (57) and integrating gives

$$\tan \gamma = \tan \gamma(0) - \frac{\lambda_3 \beta}{\cos \gamma(0)} \quad (94)$$

Combining Equations (54) and (56) and integrating gives

$$\ln \frac{\sigma}{\sigma(0)} = - \frac{\lambda_1}{2\lambda_3} \cdot (u^2 - 1) \quad (95)$$

Combining Equations (58) and (57) and integrating gives

$$\theta = \theta(0) - \frac{\lambda_4}{\lambda_3} \cdot \cos^2 \gamma(0) \left[\tan \gamma - \tan \gamma(0) \right] \quad (96)$$

The comparison between the exact and approximate solutions is presented in Table 9. The agreement is surprisingly good considering the drag is neglected. It is desirable, however, that the drag be negligible for the power-off coast to apogee.

The exact solution reaches apogee at 135.6 sec.

Complete Trajectories

With the relations derived earlier, it is easy to develop a complete trajectory from launch to apogee. The initial conditions are the launch conditions. Thereafter, the initial conditions are the end conditions from the previous segment. For comparison purposes, an approximate trajectory of 130 seconds was developed and compared with the exact. The approximate solutions were based upon the methods developed in the previous sections. The first ten seconds of the trajectory was maximum lift. The next twenty seconds was constant flight path angle with power-on. The next thirty seconds was zero angle-of-attack with power-on. The last seventy seconds was zero angle-of-attack with power-off. The exact and approximate solutions are presented in Table 10.

Next we turn our attention to optimal boost climb trajectory analysis.

SECTION IV

OPTIMAL BOOST CLIMB PERFORMANCE

The objective of this analysis is to determine the aerodynamic controls as a function of time such that a boost ascension trajectory occurs in some optimal manner. In all problems, the angle-of-attack is a control variable. In some problems, the thrust vector angle is also a control variable. When it is not, the thrust vector angle will be set equal to zero.

The optimal controls are a function of the performance payoff criterion. There are three payoffs that are of interest: the first is maximum speed, the second is minimum propellant to reach specified terminal conditions, and the third is minimum time to reach apogee. The second payoff is equivalent to maximizing the burn out weight since the weight varies linearly with time.

The relevant differential equations are Equations (54) through (57). Equation (58) can be dropped since θ is not a payoff criterion; it does not contain the control, and the other differential equations do not contain θ . Since λ_2 is a constant, Equation (55) can be replaced with its integral

$$\begin{aligned} \omega &= 1 - \lambda_2 \beta \\ &= 1 - \lambda_2 \end{aligned} \quad \begin{aligned} 0 \leq \beta \leq \frac{t_{B0}}{t_R} &= \beta_{B0} \\ \beta_{B0} \leq \beta \end{aligned} \quad (97)$$

where t_{B0} is the burnout time. It is assumed that the thrust and aerodynamic coefficients are independent of altitude and Mach number. This appears to be a gross approximation, but generally the acceleration from subsonic to hypersonic speeds is

very rapid for high thrust to weight configurations. At hypersonic speeds, the aerodynamic coefficients will be a function of only the angle-of-attack.

The boost is at maximum thrust until burnout. For some problems, this is the terminal condition. For other problems, the vehicle coasts to apogee after burnout. This corresponds to

$$\gamma(\beta_f) = 0 \quad (98)$$

The optimal trajectory problems are identified in Table 11. The solutions to Problems 4 and 9 are trivial. If the final conditions are free, then minimum propellant or minimum time is zero. Thus, the initial and final times are the same. Since the propellant used is a function of time, Problems 5, 6, 7, and 8 are equivalent to 10, 11, 12, and 13, respectively.

The following examples will be addressed later on in this section. In Problem 1, the payoff is the final speed and there are no constraints. The remaining problems are apogee problems and are defined as follows in Table 12.

Aerodynamic Relations

Since the drag and lift coefficients are respectively even and odd functions, rewrite Equations (14) and 16) as follows

$$C_D = K|\sin^3\alpha| + C_{D_0} \quad (99)$$

$$C_L = K|\sin\alpha|\sin\alpha\cos\alpha \quad (100)$$

where $|x|$ means absolute value of x . For the configuration to be used in this section, $C_{D_0} = 1.035$ and $K = 35.30$. In order to develop necessary and sufficient conditions for the optimal controls, we need first and second derivatives of C_L and C_D with respect to α . The derivatives are

$$C_{L\alpha} = K(2\cos^2\alpha - \sin^2\alpha)|\sin\alpha| \quad (101)$$

$$\begin{aligned} C_{L\alpha\alpha} &= K(2\cos^2\alpha - 7\sin^2\alpha)\cos\alpha \quad \alpha > 0 \\ &= -K(2\cos^2\alpha - 7\sin^2\alpha)\cos\alpha \quad \alpha < 0 \end{aligned} \quad (102)$$

$$C_{D\alpha} = 3C_L \quad (103)$$

$$C_{D\alpha\alpha} = 3C_{L\alpha} \quad (104)$$

The coefficients and their derivatives are presented in Figures 4 through 7. The range of α is that from $-C_{L\text{MAX}}$ to $+C_{L\text{MAX}}$.

The optimal control problem is considered next.

Optimal Control Problem

The approach to determining the solution of the optimal control problem is given in Reference 2. The optimal control problem is the maximization of the Hamiltonian with respect to the control variables. The Hamiltonian is defined as follows

$$H = P_u u' + P_\gamma \gamma' + P_\sigma \sigma' \quad (105)$$

where P_u , P_γ , P_σ are the costate variables associated with the state variables u , γ , σ . The necessary condition for a costate variable x (u , γ , or σ) on an optimal trajectory is

$$F'_x = - \frac{\partial H}{\partial x} \quad (106)$$

Consequently, three additional differential equations result.

If the thrust vector angle is free, there are three control variables. Since δ is the sum of α and δ_v , only two can be

considered as independent. The choice is α and δ_v . If the thrust vector is fixed, $\delta_v = 0$, then only α is free. Necessary conditions for both cases will be addressed. Consider first free δ_v and α . Introduce two control functions

$$F(\delta_v) = C_T(\cos\delta + P_R \sin\delta) \quad (107)$$

$$G(\alpha) = F(\alpha) - C_D + P_R C_L \quad (108)$$

where

$$\delta = \alpha + \delta_v, \quad C_T = \frac{T}{qS}, \quad P_R = \frac{P_Y}{uP_U} \quad (109)$$

The part of the Hamiltonian that is a function of δ_v is

$$H(\delta_v) = \lambda_3 P_U \cdot \frac{qS}{W} \cdot F(\delta_v) \quad (111)$$

The part of the Hamiltonian that is a function of α is

$$H(\alpha) = \lambda_3 P_U \cdot \frac{qS}{W} \cdot G(\alpha) \quad (111)$$

If δ_v is unconstrained, optimal δ_v , δ_v^* , is the solution of

$$\frac{\partial F(\delta_v)}{\partial \delta_v} = 0 \quad (112)$$

Substitution gives

$$\tan(\alpha + \delta_v^*) = P_R \quad (113)$$

If α is unconstrained, optimal α , α^* , is the solution of

$$\frac{\partial G(\alpha)}{\partial \alpha} = 0 \quad (114)$$

or

$$F_{\alpha} - C_{D_{\alpha}} + P_R C_{L_{\alpha}} = 0 \quad (115)$$

Since $F_{\alpha} = F_{\delta_v} = 0$ according to Equation (112), then α must be the solution of

$$- C_{D_{\alpha}} + P_R C_{L_{\alpha}} = 0 \quad (116)$$

Substituting Equations (103), (100), and (101) gives

$$-3\tan\alpha^* + P_R(2 - \tan^2\alpha^*) = 0 \quad (117)$$

We can solve for α^* as a function of P_R or P_R as a function of α^* . We choose the latter so that we can examine the Hamiltonian as a function of α^* and δ_v^*

$$P_R = \frac{3\tan\alpha^*}{2 - \tan^2\alpha^*} \quad (118)$$

Thus, once α^* is determined, P_R is determined from Equation (118) and δ_v^* is obtained from Equation (113). In Figure 8, P_R is presented as a function of α^* . In Figure 9, δ_v^* is presented as a function of α^* . The functions F and G , evaluated at α^* and δ_v^* , are presented in Figures 10 and 11 as functions of α^* and C_T .

In order that the Hamiltonian be a local maximum, it is necessary that

$$H_{\alpha\alpha} < 0 \quad (119)$$

and

$$H_{\delta_v\delta_v} < 0 \quad (120)$$

Both relations are evaluated for the optimal controls. In Figures 12 and 13, $F_{\delta_v \delta_v}$ and $G_{\alpha\alpha}$ are presented. Since both partial derivatives are negative, it follows from Equations (110) and (111) that along the optimal trajectory

$$P_u \geq 0 \quad (121)$$

From Equation (109) and Figure 8, it follows that if $\alpha \leq 0$, $P_R \leq 0$, therefore, $P_Y \leq 0$. If $\alpha \geq 0$, $P_R \geq 0$, therefore, $P_Y \geq 0$. Furthermore, if $\alpha = 0$, $P_Y = 0$.

If the thrust vector angle is fixed, assume $\delta_v = 0$, then along the optimal trajectory

$$G_\alpha = F_\alpha - C_{D_\alpha} + P_R C_{L_\alpha} = 0 \quad (122)$$

In this case, $F_\alpha \neq 0$. The optimal angle-of-attack is the solution of

$$C_T(-\sin\alpha^* + P_R \cos\alpha^*) - C_{D_\alpha}^* + P_R C_{L_\alpha}^* = 0 \quad (123)$$

Substituting Equations (103), (100), and (101) gives

$$\begin{aligned} C_T(-\sin\alpha^* + P_R \cos\alpha^*) - 3K|\sin\alpha^*|\sin\alpha^* \cos\alpha^* \\ + P_R K(2\cos^2\alpha^* - \sin^2\alpha^*)|\sin\alpha^*| = 0 \end{aligned} \quad (124)$$

The optimal angle-of-attack is a function of P_R , K , and C_T . Previously it was a function of only P_R . By substituting tangent trigonometric relations for sine and cosine terms, Equation (124) can be transformed to a cubic equation in $\tan\alpha^*$

$$C_T(-x + P_R)(1 + x^2) - 3K|x|x + P_R K(2 - x^2)|x| = 0 \quad (125)$$

where

$$x = \tan \alpha^* \quad (126)$$

Equation (125) can be solved for α^* as a function P_R , K , and C_T or P_R solved in terms of α^* , K , and C_T . Thus

$$P_R = \frac{C_T x(1 + x^2) + 3K|x|x}{C_T(1 + x^2) + K(2 - x^2)|x|} \quad (127)$$

P_R is presented in Figure 14. In Figure 15, $G(\alpha^*)$ is presented. $G_{\alpha\alpha}(\alpha^*)$ is presented in Figure 16.

For maximum Hamiltonian, Relation (119) must hold. From Equation (111) it follows that along the optimal trajectory

$$P_u \geq 0 \quad (128)$$

This agrees with the previous case. Thus for both situations, free or fixed thrust vector angle, Equations (121) and (128) hold.

We next turn our attention to the development of the optimal trajectory solutions.

Optimal Trajectory Solutions

There are two ways to determine the optimal trajectory. The first way involves determining the costate differential equations according to Equation (106) and then integrating these equations between appropriate boundary conditions. The second way is an extension of the first and involves developing differential equations for the controls. These equations are also a function of Equation (106).

The first approach will be employed here. Two differential equations that involve the costate variables are required. Only two are required since the costate variables can be normalized

with respect to P_u . The differential equations are in terms of P_R and P_S where

$$P_S = \frac{P_\sigma}{P_u} \quad (129)$$

From Equation (106), the differential equations are

$$P_R' = \frac{1}{u} \cdot \lambda_3 \cos \gamma - P_S \lambda_1 \sigma \cos \gamma - \frac{1}{u} \cdot \lambda_3 P_R \left(\frac{T}{W} \cdot \cos \delta + d \right) - \frac{1}{u} \cdot P_R^2 \lambda_3 \left(\frac{T}{W} \cdot \sin \delta - n - \cos \gamma \right) + P_R P_S \lambda_1 \sigma \sin \gamma \quad (130)$$

$$P_S' = \lambda_3 d \left(\frac{1}{\sigma} - \frac{2P_S}{u} \right) - \frac{1}{u} \cdot \lambda_3 n P_R \left(\frac{u}{\sigma} - P_S \right) - \lambda_1 P_S u \sin \gamma - \frac{1}{u} \cdot \lambda_3 P_S P_R \frac{T}{W} \cdot \sin \delta + \frac{1}{u} \cdot \lambda_3 P_S P_R \cos \gamma + P_S^2 \lambda_1 \sigma \sin \gamma \quad (131)$$

These equations and the trajectory equations are integrated forward in time to the burnout condition. Optimal controls are imposed everywhere along the trajectory. Initial guesses for $P_S(0)$ and $P_R(0)$ or $\alpha(0)$ are required. For problem 1, the final flight path angle and altitude are free, thus

$$P_S(t_f) = 0 \quad P_R(t_f) = 0 \quad (132)$$

Results are presented in Figures 17 through 23. The differences for free δ_v or $\delta_v = 0$ are negligible for the speed and altitude. The payoffs for Problem 1 are presented in Table 13. Since the difference in the speed for the first problem is negligible, the remaining problems will be constrained by $\delta_v = 0$.

For problems 2, 3, and 4, the optimal trajectory solutions are presented in Figures 24 through 27. The initial values for α^* and P_S are presented in Table 14 along with the constraints and optimal payoff. For reference purposes, the maximum speed for Problem 1 and $\delta_v = 0$ is $V(t_f) = 6583$ ft/sec and $t_f = 60$

seconds. The maximum speeds for Problems 2 and 3 are less than Problem 1. Also, the speeds for Problem 3 are less than Problem 2. The minimum time solutions for Problems 4 are less than the corresponding maximum speeds for Problem 3. The flight path angle solutions show that the minimum time solution pitches up to a higher flight path angle. Once this is reached, the optimal angle-of-attack solution shows that there is a rapid pitch over until the angle-of-attack for $-C_{L_{MAX}}$ is reached. This angle-of-attack is followed until apogee is reached. This is one of the primary differences between the controls in the two problems. For minimum time to apogee, the initial pitch up is faster and the pitch down is also rapid until $-C_{L_{MAX}}$ is reached. Recall that the angle-of-attack was limited to angles between $-C_{L_{MAX}}$ and $+C_{L_{MAX}}$. A second difference is that the minimum time trajectory may reach apogee before burnout, whereas, the maximum speed solution at apogee never occurs before burnout; it must occur at or later than burnout.

SECTION V

CONCLUSIONS

Nominal and optimal boost climb trajectories were developed for an air launched vehicle. The approximate nominal solutions were in good agreement with the solutions obtained by numerical integration of the differential equations of motion. The advantage of the approximate solutions is a rapid estimate of the ascent of a rocket powered vehicle.

For the optimal trajectories, three payoffs were considered; maximum speed at burnout or apogee, minimum fuel to apogee, and minimum time to apogee. The last two problems are equivalent since the fuel burning rate is constant. Thrust vectoring was considered, but the difference relative to no vectoring was negligible for the problem of maximizing the speed at burnout. As a result, all subsequent problems assumed no thrust vectoring.

In general, the optimal angle-of-attack decreased with increasing time. The change was greater for the minimum time solution. For this case, a fast pitch up occurred initially and then the angle-of-attack rapidly decreased to the angle-of-attack for $-C_{L_{MAX}}$. This gave the fastest pitch over to apogee.

The minimum time solution may reach apogee before burnout. The emphasis is on reaching apogee before burning all propellant. For the problem of maximum speed at apogee, all propellant is used prior to or at apogee. The reason for this is that as long as there is propellant, the vehicle will continue to accelerate.

The analysis has been limited to constant thrust and burning rate and a single booster. If the constants are variable, then relationships as a function of the appropriate variables

must be included. This will change the costate differential equations if the engine variables are dependent upon any of the state variables. If there is more than one booster, there may be coast period between boosts. Care must be exercised to insure that this possibility is properly accounted for.

REFERENCES

1. Hankey, W. L., "Optimization of Lifting Re-entry Vehicles," ASD-TDR-62-1102, March 1963, Wright-Patterson AFB, Ohio.
2. Vinh, N. X., "Optimal Trajectories in Atmospheric Flight," Elsevier Scientific Publishing Company, Amsterdam - Oxford - New York, 1981.
3. Gord, P. R., and Brigalli, A. J., "X24C-10D Force and Moment Test Results at Mach Numbers from 0.4 to 8.0," AFFDL-TM-78-3 FXG, Jan 1978, Flight Dynamics Laboratory, Wright-Patterson AFB, Ohio.
4. Dahlem, Valentine III, "Static Aerodynamic Characteristics of Three Blunt Elliptical Bodies at Subsonic to Hypersonic Speeds," FDMG TM 64-23, Flight Dynamics Laboratory, Jun 1964.
5. "Aerodynamic Design Data Book, Volume 1, Orbiter Vehicle 102," SD72-SH-0060, Volume 1L, Rockwell, October 1978.
6. Dahlem, Valentine III, Johnson, D. T., and Willbanks, H. III, "Experimental and Analytical Study of Two Advanced Manned Interceptor Configurations from Mach 0.2 to 6.0," AFFDL-TR-74-14, April 1974, Flight Dynamics Laboratory, Wright-Patterson AFB, Ohio.
7. "Aerodynamic Stability and Control Data, Model 844-2050," D2-80065, Boeing, May 1965.
8. Kinroth, G. D., and Pawlikowski, T. P., "ASSET, Volume III. Final Aerodynamics and Performance," AFFDL TR-65-31 Volume III, December 1965, Flight Dynamics Laboratory, Wright-Patterson AFB, Ohio.

9. Hankey, W. L., and Elliott, G. A., "Hypersonic Lifting Body Optimization," ARL 69-0056, May 1969, Aerospace Research Laboratories, Wright-Patterson AFB, Ohio.

APPENDIX

CORRELATION BETWEEN EXPERIMENTAL AND THEORETICAL AERODYNAMIC DATA

Seven different configurations were examined. Maximum lift-to-drag ratio varied from approximately one to over four. The seven configurations are the X24C, Reference 3, Super Orbital Re-entry Test Integrated Environment (SORTIE), Reference 4, Shuttle Orbiter Vehicle 102, Reference 5, Advanced Manned Interceptor (AMI), Reference 6, X20 Dynasoar, Reference 7, Aerothermodynamic/Elastic Structural Systems Environmental Tests (ASSET), Reference 8, and an optimized configuration from Reference 9. The configurations are illustrated in Figure A-1 where the AMI has the highest experimental maximum L/D ratio and the SORTIE is the lowest. In all but the optimized configuration, either C_L and C_D , or C_N and C_A were available. If the latter were available, then the data were transformed to C_L and C_D . For the optimized configurations, only L/D distributions were available.

The experimental data were obtained from wind tunnel tests. The theoretical distribution were assumed to correspond to the relations in Section II, Equations (14) and (16)

$$C_L = K \sin^2 \delta \cos \delta \quad (14)$$

$$C_D = K \sin^3 \delta + C_{D_0} \quad (16)$$

It will be assumed that

$$\delta = \alpha + \alpha_0 \quad (17)$$

There are different ways for correlating the data. The approach here was to determine K , C_{D_0} , and α_0 such that a satisfactory fit to L/D and C_L was obtained. For each data set, a

subset of the data was selected. The error is defined as follows

$$\begin{aligned} \text{ERROR} &= \sum_{i=N_1}^{N_2} \left\{ \left[E(\text{theor}) - E(\text{exp}) \right]^2 + \left[C_L(\text{theor}) - C_L(\text{exp}) \right]^2 \right\} \\ &= \sum_{i=N_1}^{N_2} \left\{ \left[\frac{\sin^2 \delta \cos \delta}{\sin^3 \delta + C} - E(\text{exp}) \right]^2 + \left[K \sin^2 \delta \cos \delta - C_L(\text{exp}) \right]^2 \right\} \end{aligned} \quad (\text{A-1})$$

where N_1 is the first point and N_2 is the last point. The objective was to minimize the error with respect to the parameters C and K . The parameter C was obtained from the minimization of the squared error between the theoretical and experimental values for L/D and was accomplished by employing a golden section search technique. The minimization of the error with respect to K was obtained by minimizing the error in C_L . For the optimized configuration only C was obtained. For all but this configuration, α_0 was assumed to be zero. For this configuration it appeared that $\alpha_0 = 4^\circ$ gave the best fit to the data.

The results are presented in Figures A-2 through A-8. The emphasis was on a satisfactory fit to the L/D data in the neighborhood of E^* . Consequently, some of the data does not fit well at larger angles-of-attack. If maneuvers at large angles-of-attack are required, then the emphasis should be on the region of interest. It can be seen that the experimental and theoretical distributions match quite well in the neighborhood of E^* .

The values of N (total number of experimental points), N_1 , N_2 , C_{D_0} , K , δ^* , and E^* are presented in Table A. The solutions

for δ^* and E^* were obtained from Equations (20) and (23). For the optimum vehicle, it was assumed that $E^* = 3$, $\alpha_0 = 4^\circ$, and δ^* and C were computed from Equations (24) and (21). for the purpose of this investigation, the theoretical distributions for C_L and C_D are satisfactory.

Table 1

ATMOSPHERIC PARAMETERS

	<u>A</u>	<u>B</u>
$0 \leq h \leq 25,000$ feet	0.9858×10^{-2}	-0.3209×10^{-4}
$25,000 < h < 150,000$ feet	0.4231	-0.4695×10^{-4}
$150,000 \leq h < 250,000$ feet	-0.6150	-0.3956×10^{-4}
$250,000 \leq h$	3.734	-0.5704×10^{-4}

Table 2

EXPONENTIAL DENSITY ERRORS

Altitude <u>(ft)</u>	Error <u>(%)</u>
0	-1.0
25,000	-1.0
50,000	4.1
75,000	-3.7
100,000	-1.3
125,000	-3.4
150,000	-3.0
175,000	-0.8
200,000	3.9
225,000	5.8
250,000	-4.4
275,000	1.8
300,000	-3.1

Table 3

AERODYNAMIC PARAMETERS

E^*	δ^* (Deg)	C_D / K	$C_D(\delta^*) / C_{D_0}$
1	29.32	.0916	2.28
2	17.57	.0159	2.73
3	12.24	.0051	2.86
4	9.34	.0021	2.92

Table 4

EXACT AND APPROXIMATE AERODYNAMIC PARAMETERS

EXACT				APPROXIMATE		
C_{D_0} / K	E^*	C_L^* / K	C_D^* / C_{D_0}	E^*	C_L^* / K	C_D^* / C_{D_0}
0.3675	0.5	0.320	1.74	0.74	0.814	3
0.0916	1.0	0.209	2.28	1.17	0.323	3
0.0342	1.5	0.132	2.57	1.63	0.167	3
0.0159	2.0	0.087	2.73	2.10	0.100	3
0.0051	3.0	0.044	2.86	3.07	0.047	3
0.0022	4.0	0.026	2.92	4.05	0.027	3

Table 5

SAMPLE BOOSTER PROPULSION CHARACTERISTICS

<u>Booster</u>	<u>T/W(0)</u>	<u>t_B(sec)</u>	<u>ΔV(ft/sec)</u>	<u>W_{PROP}/W(0)</u>
1	2.58	38.8	4200	0.44
2	2.94	3.9	5300	0.54
3	15.69	5.4	3500	0.40
4	18.40	3.2	2400	0.30
5	1.87	28.9	2100	0.31
6	3.75	26.9	4300	0.45
7	20.17	4.3	3600	0.40
8	9.42	5.5	1900	0.25
9	21.41	3.4	2800	0.31
10	16.40	3.0	1800	0.20
11	2.18	60.0	5900	0.49
12	2.84	60.0	8900	0.64
13	2.66	59.3	9900	0.68
14	3.00	60.1	9500	0.67
15	2.54	60.1	7200	0.56
16	2.71	59.0	7700	0.58
17	2.51	60.0	8200	0.69

Table 6

INITIAL ROTATION RESULTS

$$V(0) = 700 \text{ ft/sec}, \gamma(0) = 0^{\circ}, h(0) = 40,000 \text{ ft}, \theta(0) = 0^{\circ},$$

$$W(0) = 14,997 \text{ lbs}, \dot{W} = 172.5 \text{ lb/sec}, g = 32.174 \text{ ft/sec}^2,$$

$$R = 20,925,780 \text{ ft}, T = 37,600 \text{ lb}, C_D(0) = 2.115, C_L(0) = 6.920,$$

$$t_R = 10.0 \text{ sec}, \delta = 25^{\circ}, S = 10.9 \text{ ft}^2$$

<u>EXACT</u>					<u>APPROXIMATE</u>			
<u>t</u>	<u>V</u>	<u>γ</u>	<u>h</u>	<u>θ</u>	<u>V</u>	<u>γ</u>	<u>h</u>	<u>θ</u>
0	700	0	40,000	0	700	0	40,000	0
1	765	2.18	40,000	.0020	766	2.01	40,000	.0020
2	828	4.56	40,100	.0042	831	4.22	40,100	.0042
3	889	7.13	40,100	.0065	895	6.64	40,100	.0067
4	948	9.88	40,300	.0090	958	9.27	40,300	.0093
5	1004	12.79	40,500	.0116	1020	12.11	40,500	.0122
6	1058	15.84	40,700	.0143	1081	15.16	40,700	.0152
7	1109	19.03	40,100	.0172	1141	18.43	41,100	.0185
8	1158	22.34	41,500	.0201	1199	21.92	41,500	.0220
9	1204	25.75	41,900	.0230	1256	25.62	42,100	.0258
10	1248	29.25	42,500	.0260	1311	29.54	42,800	.0297

Table 7

CONSTANT FLIGHT PATH, POWER-ON COMPARISONS

The conditions from the exact solution at the end of the initial pitch-up, $t = 10$ seconds, are the beginning of the constant flight path, power-on trajectory.

$$V(0) = 1248 \text{ ft/sec}, \gamma_c = 29.25^\circ, h(0) = 42,500 \text{ ft}, \theta(0) = .026^\circ$$

$$W(0) = 13,272 \text{ lb}, \dot{W} = 172.5 \text{ lb/sec}, T = 37,600 \text{ lb}, t_R = 50 \text{ sec}$$

$$\delta = 0, C_D(0) = 0.95, S = 10.9 \text{ ft}^2$$

<u>EXACT</u>				<u>APPROXIMATE</u>		
<u>Δt</u>	<u>V</u>	<u>h</u>	<u>θ</u>	<u>V</u>	<u>h</u>	<u>θ</u>
0	1248	42,500	.026	1248	42,500	.026
10	1903	50,300	.063	1958	50,300	.064
20	2690	61,800	.117	2809	61,900	.121
30	3701	77,600	.192	3855	78,000	.200
40	5089	99,400	.295	5190	100,000	.307
50	7095	129,500	.437	7044	130,000	.453

Table 8

ZERO ANGLE-OF-ATTACK, POWER-ON COMPARISONS

The conditions from the exact solution at $t = 30$ seconds are the initial conditions for the zero angle-of-attack, power-on trajectory.

$$V(0) = 2707 \text{ ft/sec}, \gamma(0) = 30^\circ, h(0) = 62,000 \text{ ft}, \theta(0) = 0.118^\circ, \\ W(0) = 9787.5 \text{ lb}, \dot{W} = 172.5 \text{ lb/sec}, C_D(0) = 0.75, S = 10.9 \text{ ft}^2,$$

$$T = 38,500 \text{ lb}, \alpha = 0, t_R = 30 \text{ sec}$$

<u>EXACT</u>					<u>APPROXIMATE</u>			
<u>Δt</u>	<u>V</u>	<u>γ</u>	<u>h</u>	<u>θ</u>	<u>V</u>	<u>γ</u>	<u>h</u>	<u>θ</u>
0	2707	30.0	62,000	0.118	2707	30.0	62,000	0.118
5	3193	27.3	69,100	0.154	3268	26.9	69,400	0.159
10	3753	24.9	76,700	0.196	3886	24.3	77,300	0.208
15	4405	23.0	84,900	0.247	4573	22.1	85,900	0.266
20	5173	21.2	93,900	0.307	5349	20.3	95,000	0.333
25	6087	19.8	103,700	0.379	6238	18.7	104,800	0.413
30	7193	18.6	114,600	0.464	7281	17.3	115,400	0.504

Table 9

ZERO ANGLE-OF-ATTACK POWER-OFF COMPARISONS

The initial conditions correspond to the exact solution at burnout, $t = 60$ seconds.

$$V(0) = 7193 \text{ ft/sec}, \gamma(0) = 18.6^\circ, h(0) = 117,400 \text{ ft}, \theta(0) = 0.464^\circ$$

$$W = 4612 \text{ pounds}, \alpha = 0, t_R = 70 \text{ sec.}$$

<u>EXACT</u>					<u>APPROXIMATE</u>				
<u>Δt</u>	<u>V</u>	<u>γ</u>	<u>h</u>	<u>θ</u>	<u>V</u>	<u>γ</u>	<u>h</u>	<u>θ</u>	
0	7193	18.6	114,600	0.464	7193	18.6	114,600	0.464	
10	6990	16.3	135,800	0.648	7097	16.1	135,900	0.651	
20	6863	13.9	153,800	0.830	7014	13.6	154,100	0.837	
30	6770	11.5	168,900	1.010	6946	11.0	169,000	1.023	
40	6699	9.0	180,900	1.190	6891	8.4	180,600	1.210	
50	6646	6.5	189,900	1.369	6852	5.7	189,100	1.397	
60	6609	4.0	196,000	1.548	6827	3.1	194,300	1.583	
70	6588	1.4	199,100	1.727	6817	0.4	196,400	1.770	

The exact solution reaches apogee at 135.6 sec.

$$V = 6582 \text{ ft/sec}$$

$$h = 199,600 \text{ ft}$$

$$\theta = 1.827^\circ$$

The approximate solution reaches apogee at $t = 131.3$ sec.

$$V = 6817 \text{ ft/sec}$$

$$h = 196,400 \text{ ft}$$

$$\theta = 1.795^\circ$$

Table 10

COMPLETE TRAJECTORY COMPARISONS

<u>EXACT</u>					<u>APPROXIMATE</u>			
<u>t</u>	<u>V</u>	<u>γ</u>	<u>h</u>	<u>θ</u>	<u>V</u>	<u>γ</u>	<u>h</u>	<u>θ</u>
0	700	0	40,000	0	700	0	40,000	0
10	1248	29.2	42,500	0.026	1311	29.5	42,800	0.030
30	2690	29.2	61,800	0.117	2862	29.5	62,900	0.127
60	7193	18.6	114,600	0.464	7376	17.3	117,500	0.524
130	6580	1.4	199,100	1.727	7043	-0.5	192,200	1.873

Table 11

OPTIMAL CONTROL PROBLEMS

<u>PROBLEM</u>	<u>MAXIMUM PAYOFF</u>	<u>CONSTRAINTS</u>
1	$V(t_f)$	none
2	$V(t_f)$	$\gamma(t_f) = 0$
3	$V(t_f)$	$\gamma(t_f) = 0, h(t_f)$ specified
4	$W(t_f)$	none
5	$W(t_f)$	$\gamma(t_f) = 0$
6	$W(t_f)$	$\gamma(t_f) = 0, h(t_f)$ specified
7	$W(t_f)$	$\gamma(t_f) = 0, V(t_f)$ specified
8	$W(t_f)$	$\gamma(t_f) = 0, V(t_f)$ & $h(t_f)$ specified
9	$-t_f$	none
10	$-t_f$	$\gamma(t_f) = 0$
11	$-t_f$	$\gamma(t_f) = 0, h(t_f)$ specified
12	$-t_f$	$\gamma(t_f) = 0, V(t_f)$ specified
13	$-t_f$	$\gamma(t_f) = 0, V(t_f)$ & $h(t_f)$ specified

Table 12

SELECTED OPTIMAL CONTROL PROBLEMS

$$\gamma(t_f) = 0$$

<u>PROBLEM</u>	<u>PAYOFF</u>	<u>CONSTRAINT</u>
2	$V(t_f)$	none
3	$V(t_f)$	$h(t_f)$
4	$-t_f$	$h(t_f)$

Table 13

PROBLEM 1 RESULTS

<u>δ_v</u>	<u>$V^*(t_f)$</u>	<u>$\alpha^*(0)$</u>	<u>$P_s^*(0)$</u>
free	6609 ft/sec	31.9°	-5.80
0	6583 ft/sec	34.8°	-5.34

Table 14

OPTIMAL TRAJECTORY RESULTS

<u>Problem</u>	<u>$\alpha^*(0)$</u>	<u>$P_S^*(0)$</u>	<u>Payoff</u>	<u>t_f(SEC)</u>	<u>Constraint</u>
2	35.86	-6.601	$V(t_f)=6256\text{ft/sec}$	60	none
3a	36.05	-6.555	$=6235\text{ft/sec}$	60.4	$h(t_f)=100,000\text{ft}$
3b	35.95	-6.093	$=5935\text{ft/sec}$	99.9	$=150,000\text{ft}$
4a	40.20	-7.732	$t_f=48.7\text{sec}$	----	$=100,000\text{ft}$
4b	39.30	-6.331	$=74.3\text{sec}$	----	$=150,000\text{ft}$

Table A

AERODYNAMIC PARAMETERS

<u>Vehicle</u>	<u>N</u>	<u>N_1</u>	<u>N_2</u>	<u>C_{D_0}</u>	<u>K</u>	<u>δ^*(Deg)</u>	<u>E^*</u>
AMI	5	3	3	.0081	4.279	8.86	4.23
OPTIMUM	6	-	-	-	-	12.25	3.00
X24C	7	4	5	.0222	2.705	14.29	2.54
DYNASOAR	7	3	3	.0488	2.411	19.06	1.83
SHUTTLE	11	1	11	.0543	2.821	18.77	1.86
ASSET	6	3	3	.1276	3.303	23.43	1.43
SORTIE	7	5	7	.1181	1.581	29.11	1.09

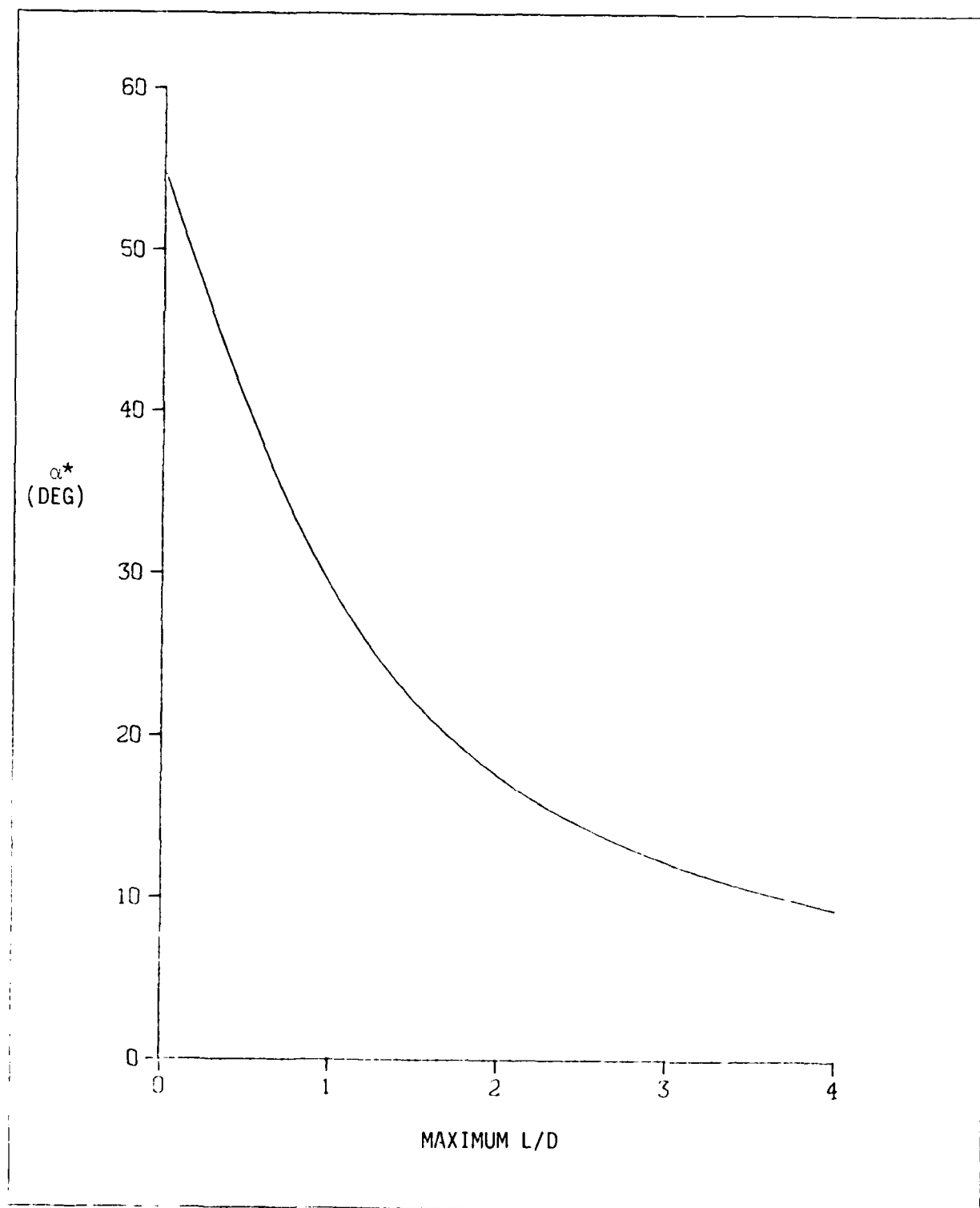


Figure 1. Optimum Angle of Attack

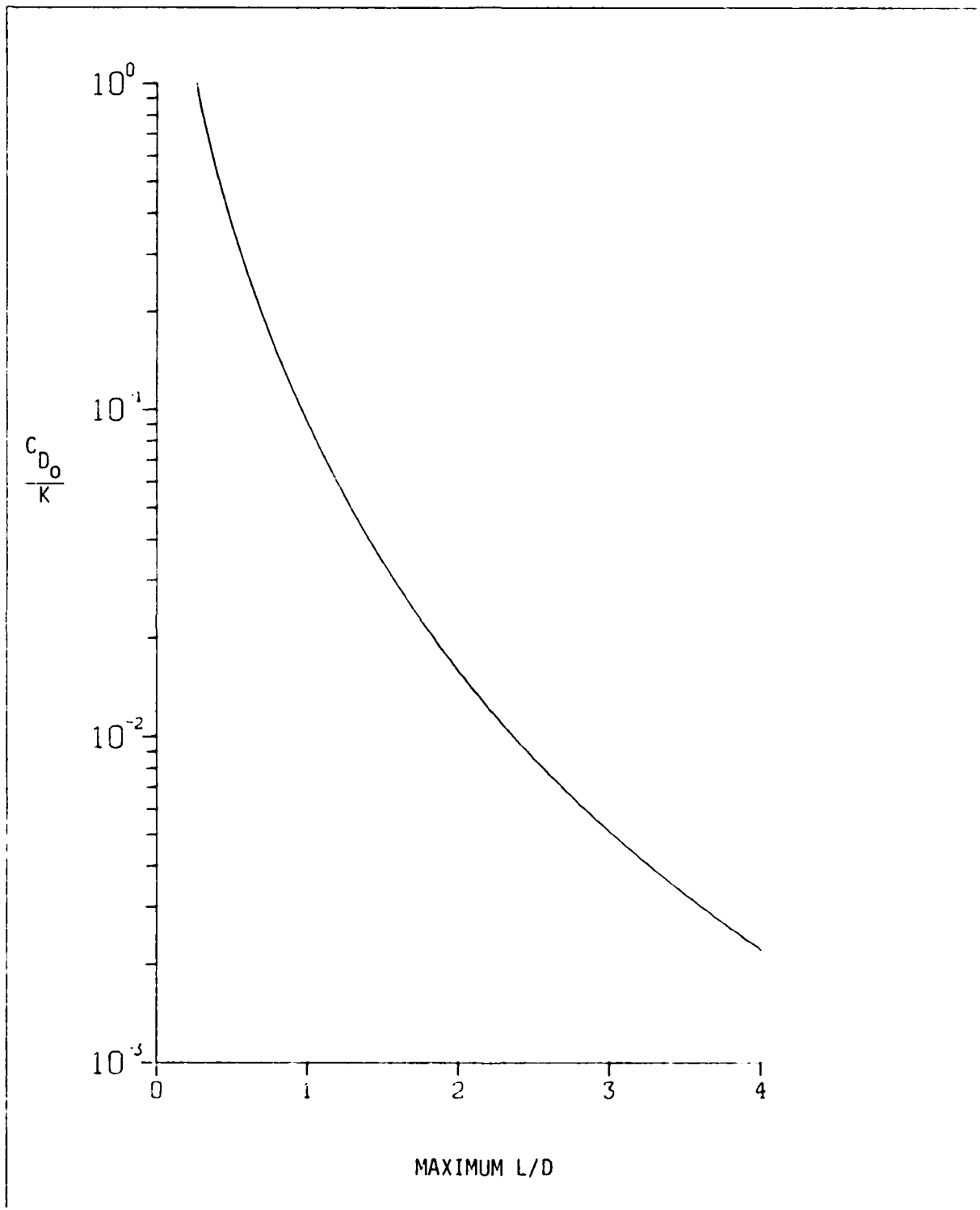


Figure 2. $\frac{C_{D_0}}{K}$

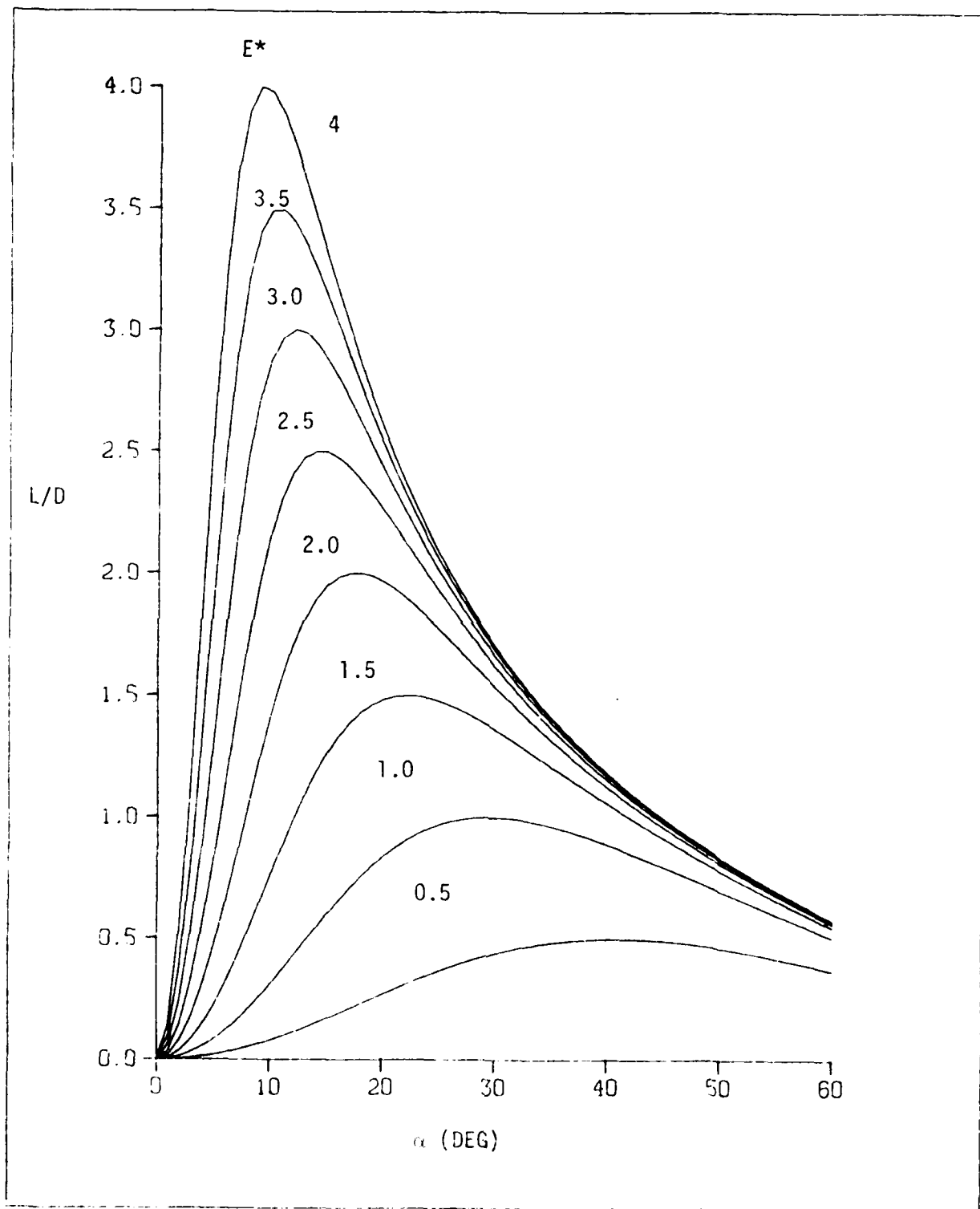


Figure 3. Lift to Drag Ratio

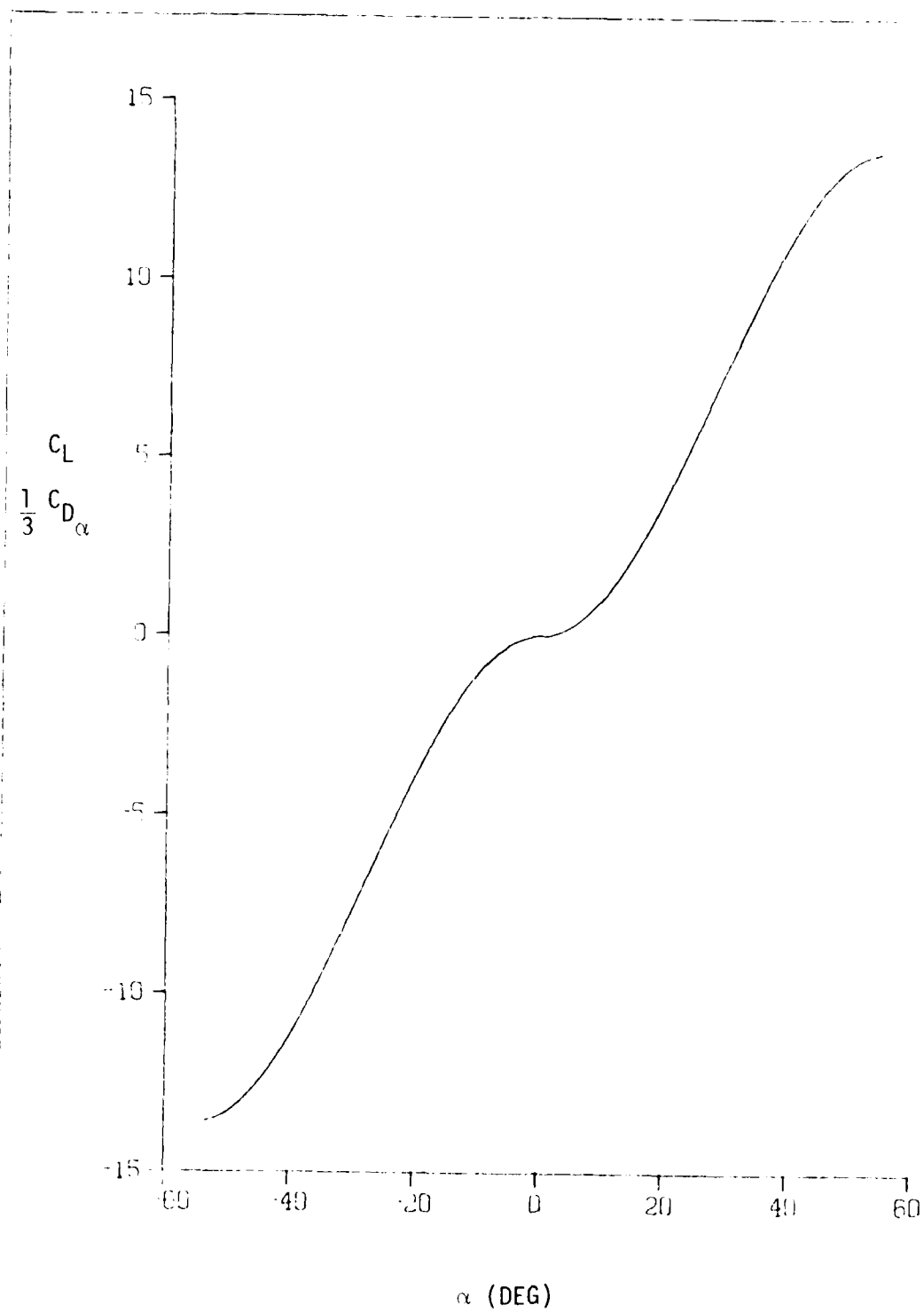


Figure 4. $C_L(\alpha)$, $\frac{1}{3} C_{D_\alpha}(\alpha)$

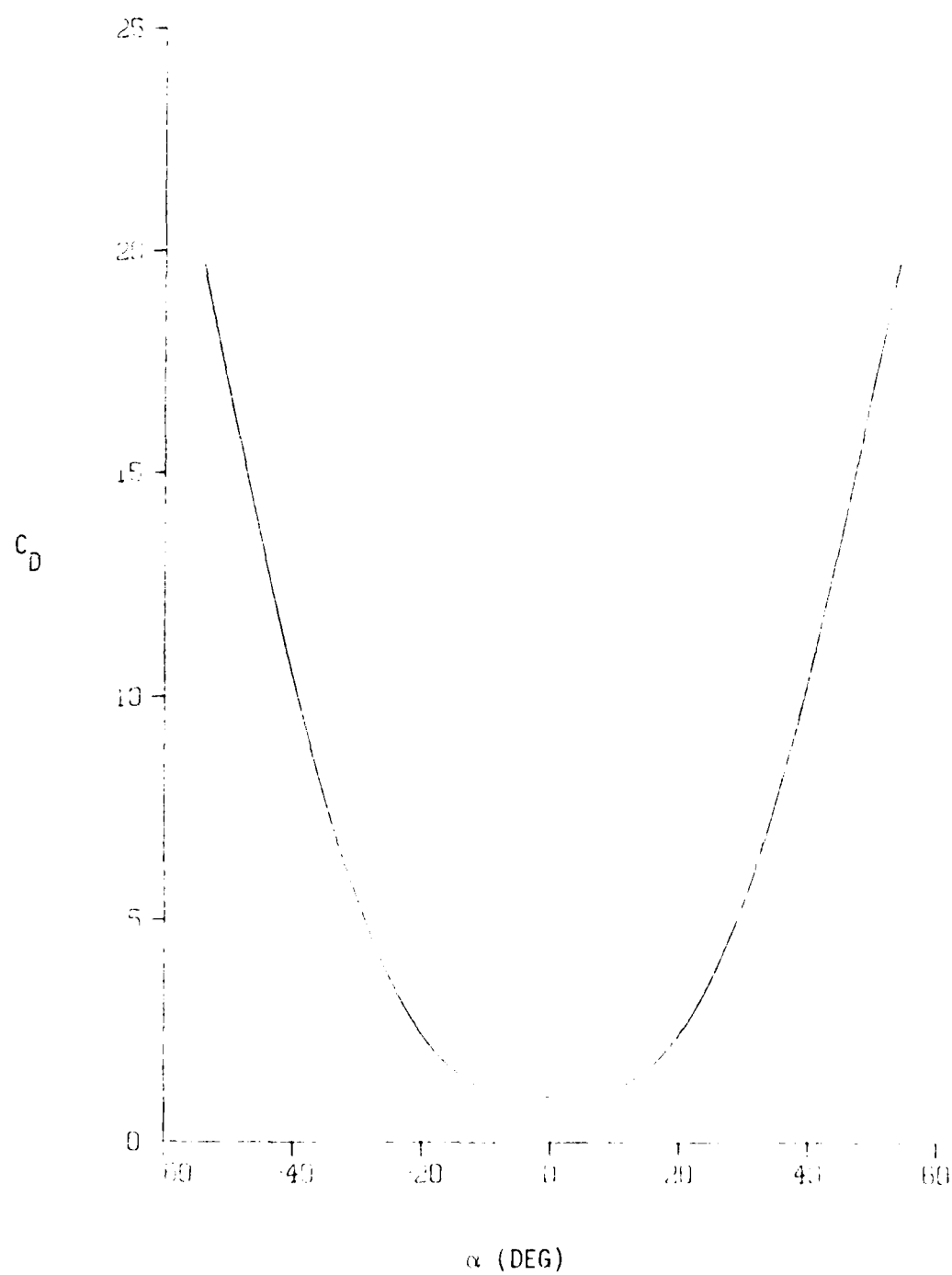


Figure 5. $C_D (\alpha)$

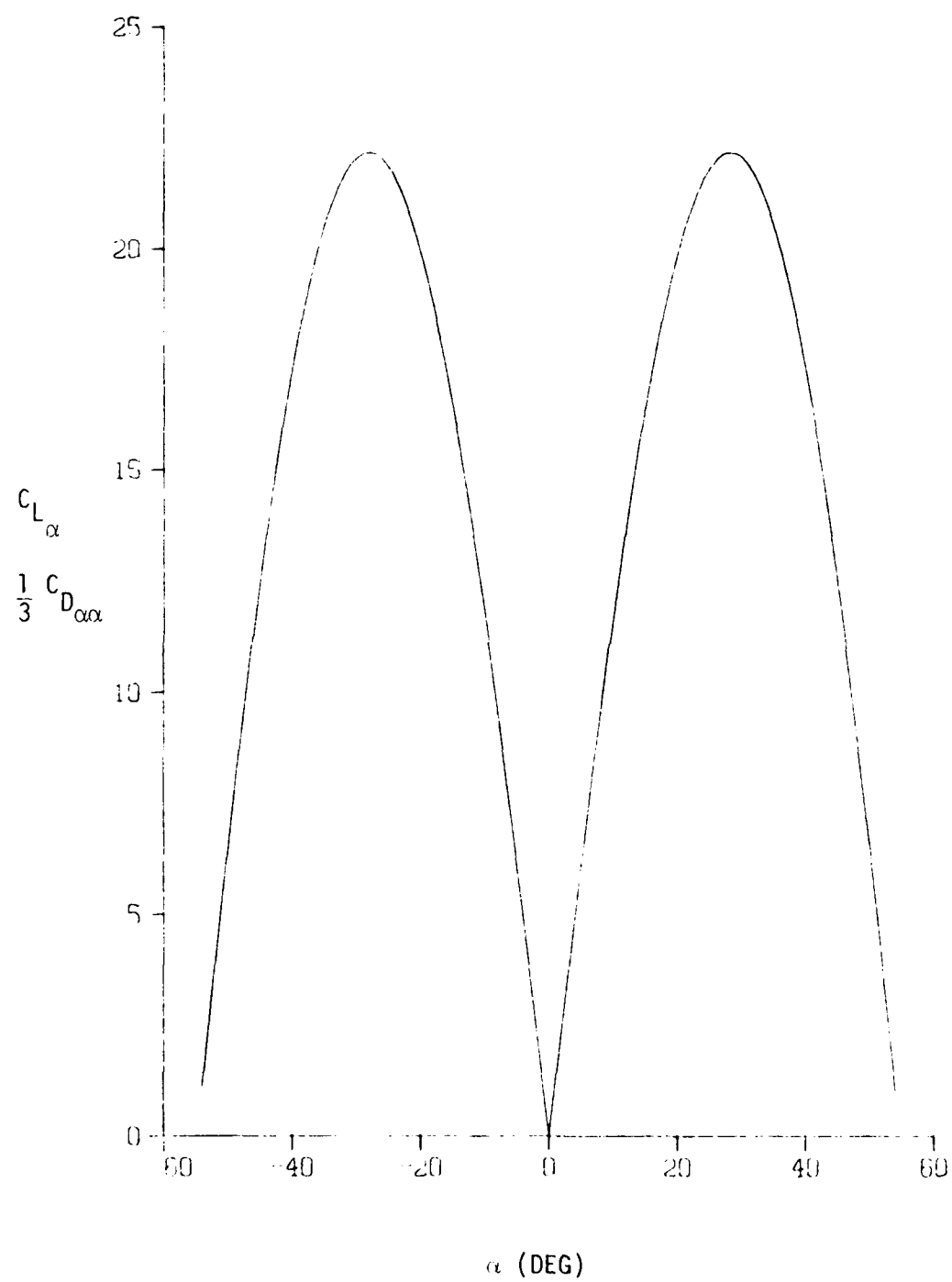


Figure 6. $C_{L_\alpha}(\alpha)$, $\frac{1}{3} C_{D_{\alpha\alpha}}(\alpha)$

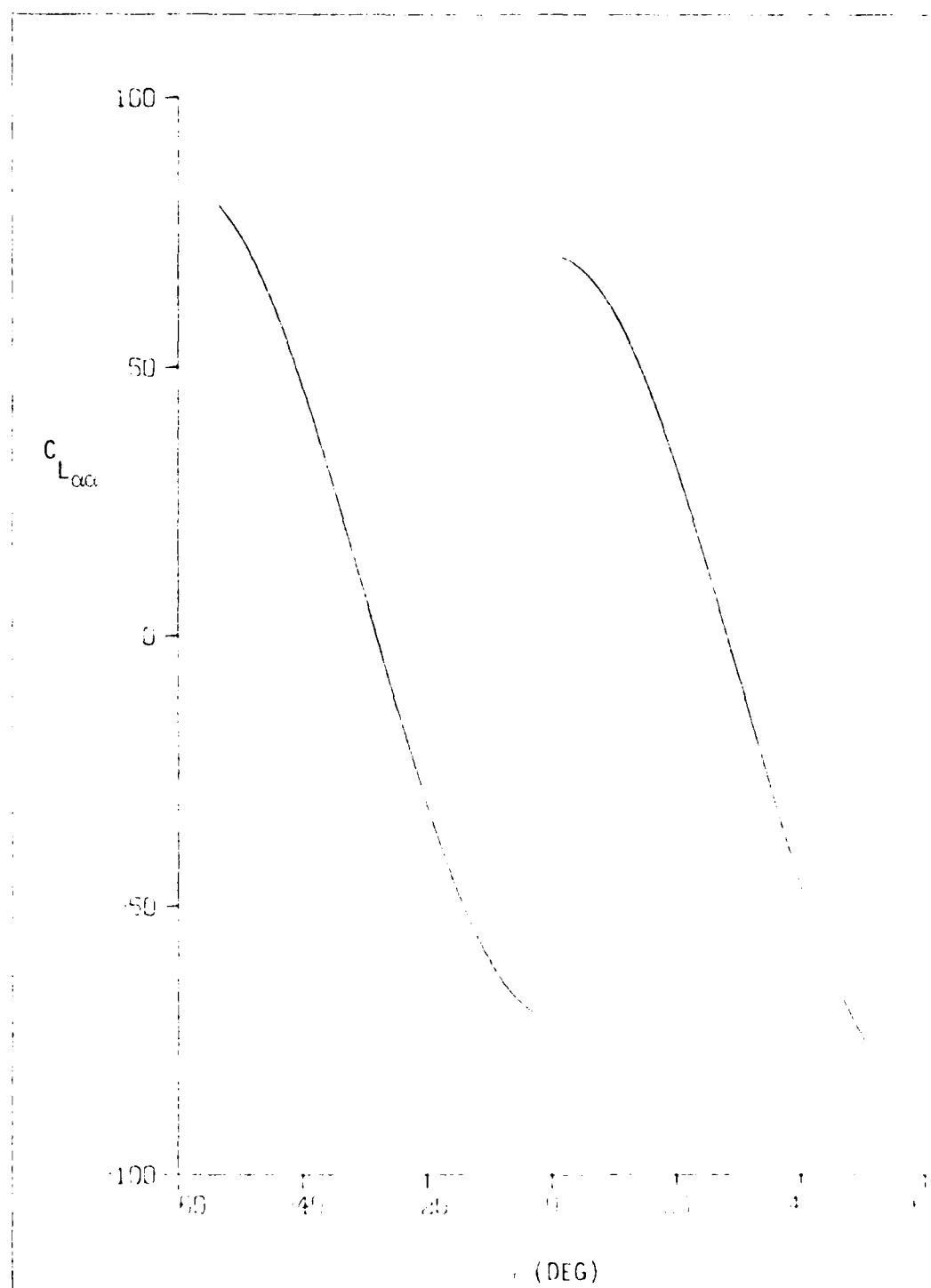


Figure 7. $C_{L_{\alpha\alpha}}$ (—)

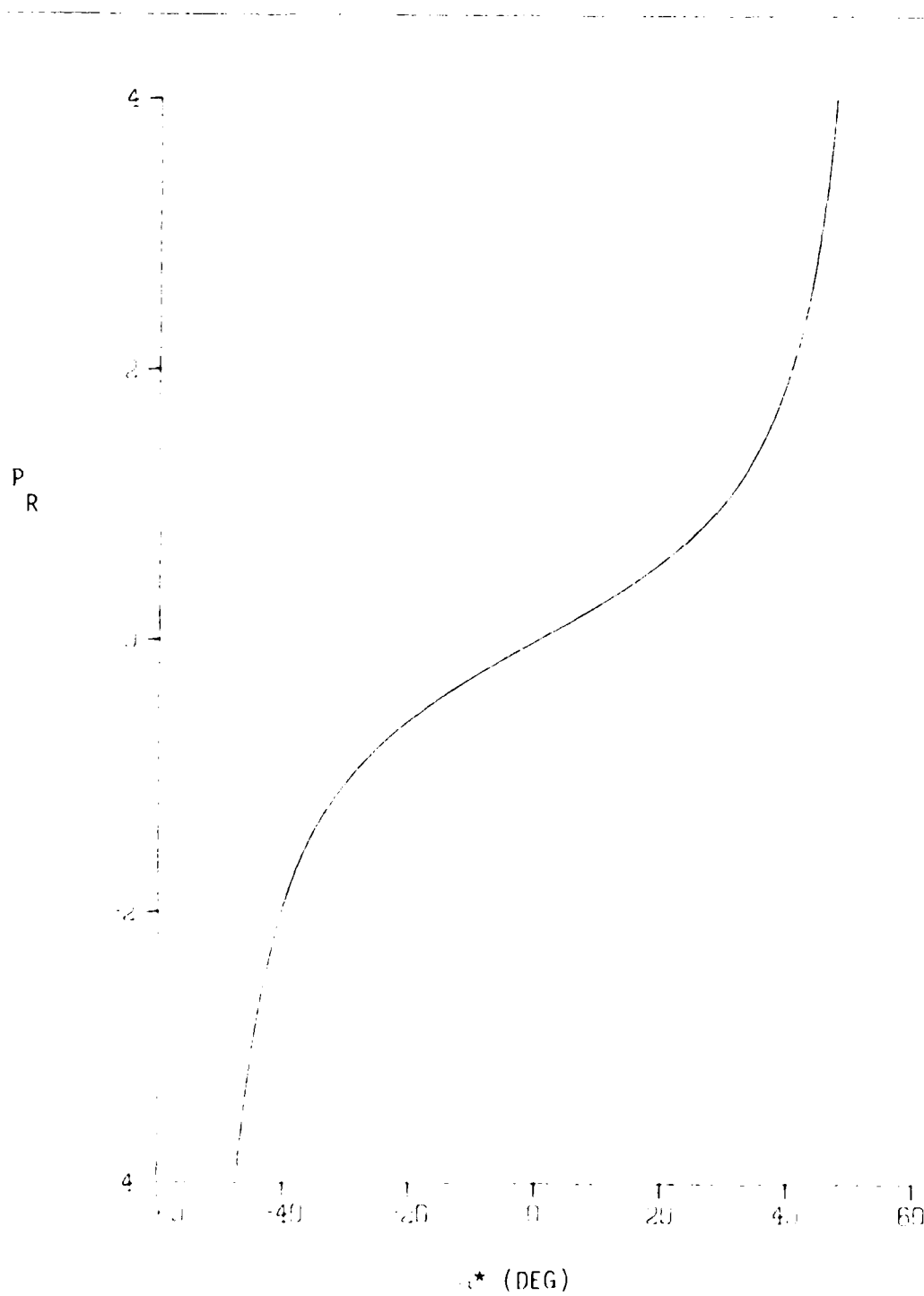


Figure 8. $P_R (\theta^*)$

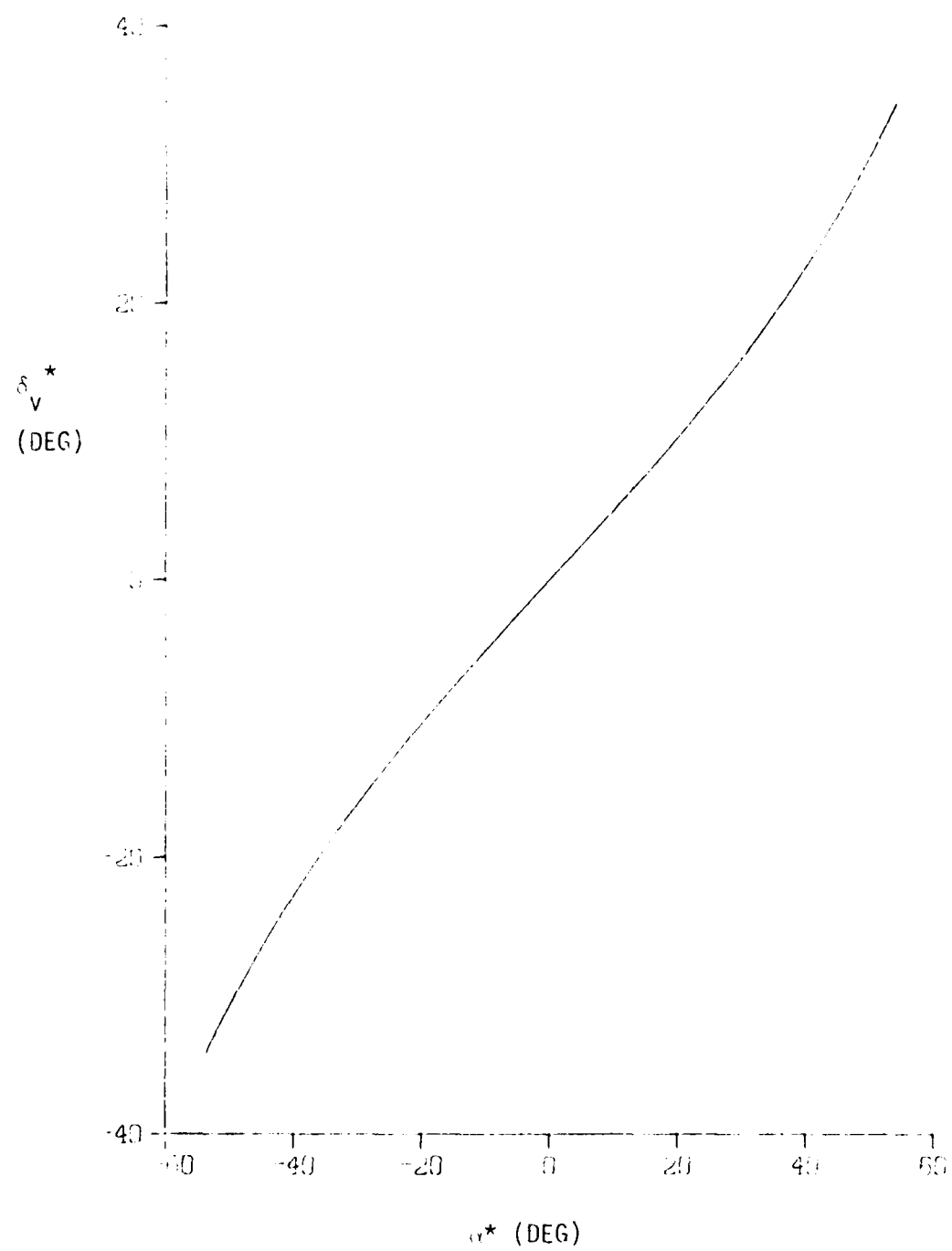


Figure 9. δ_v^* (α^*)

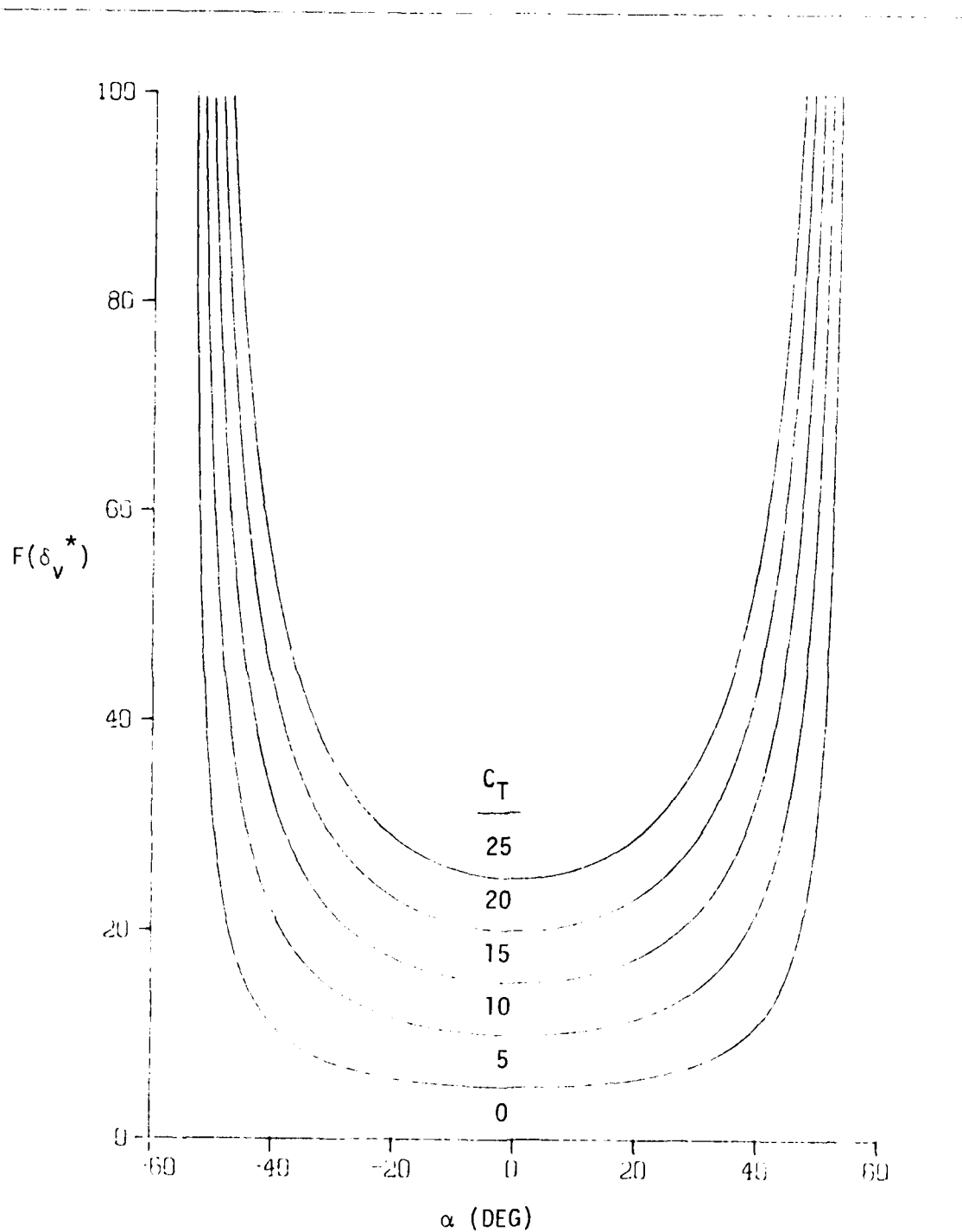


Figure 10. $F(\delta_v^*)$

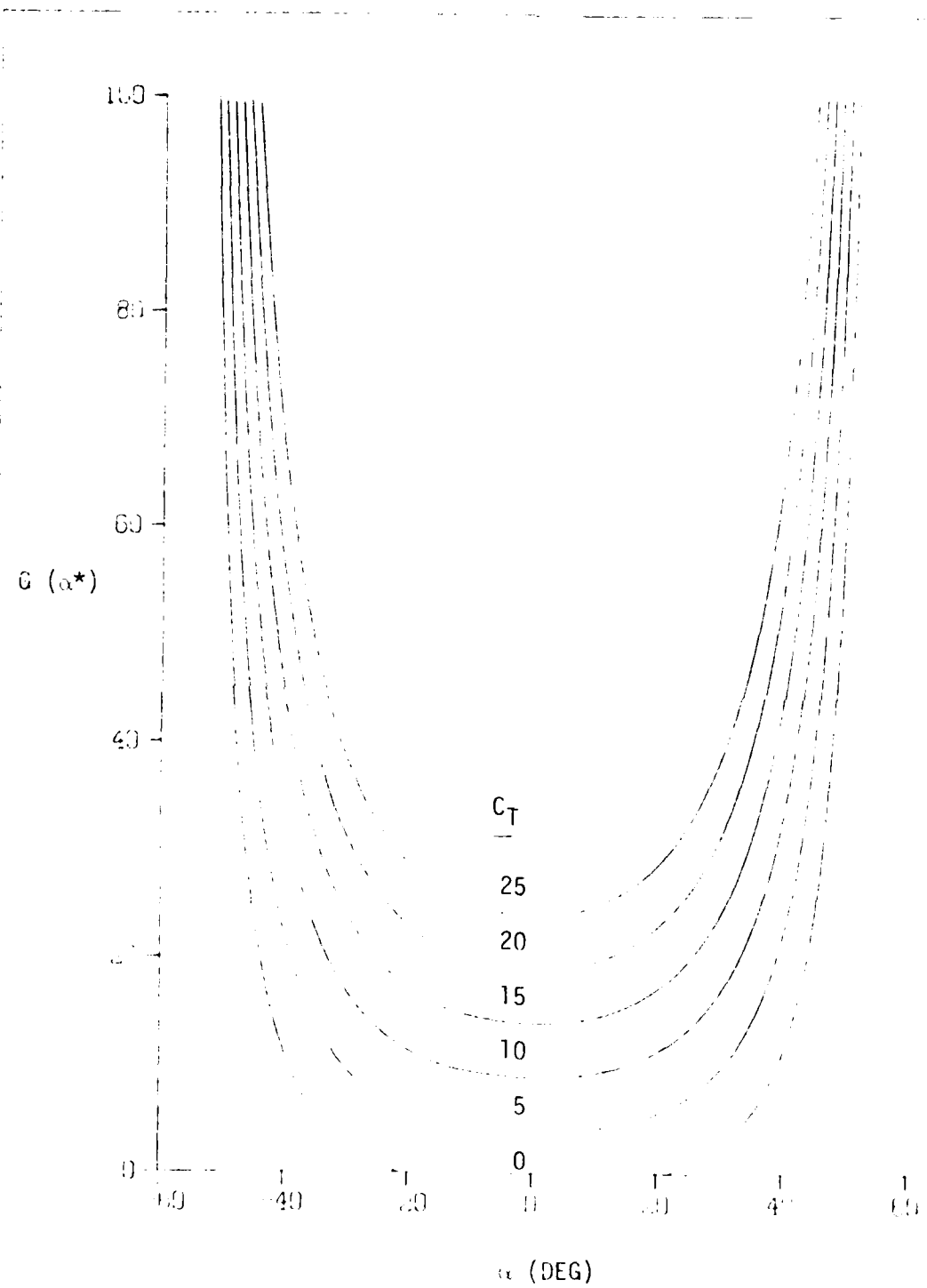


Figure 11. $G(\alpha^*)$

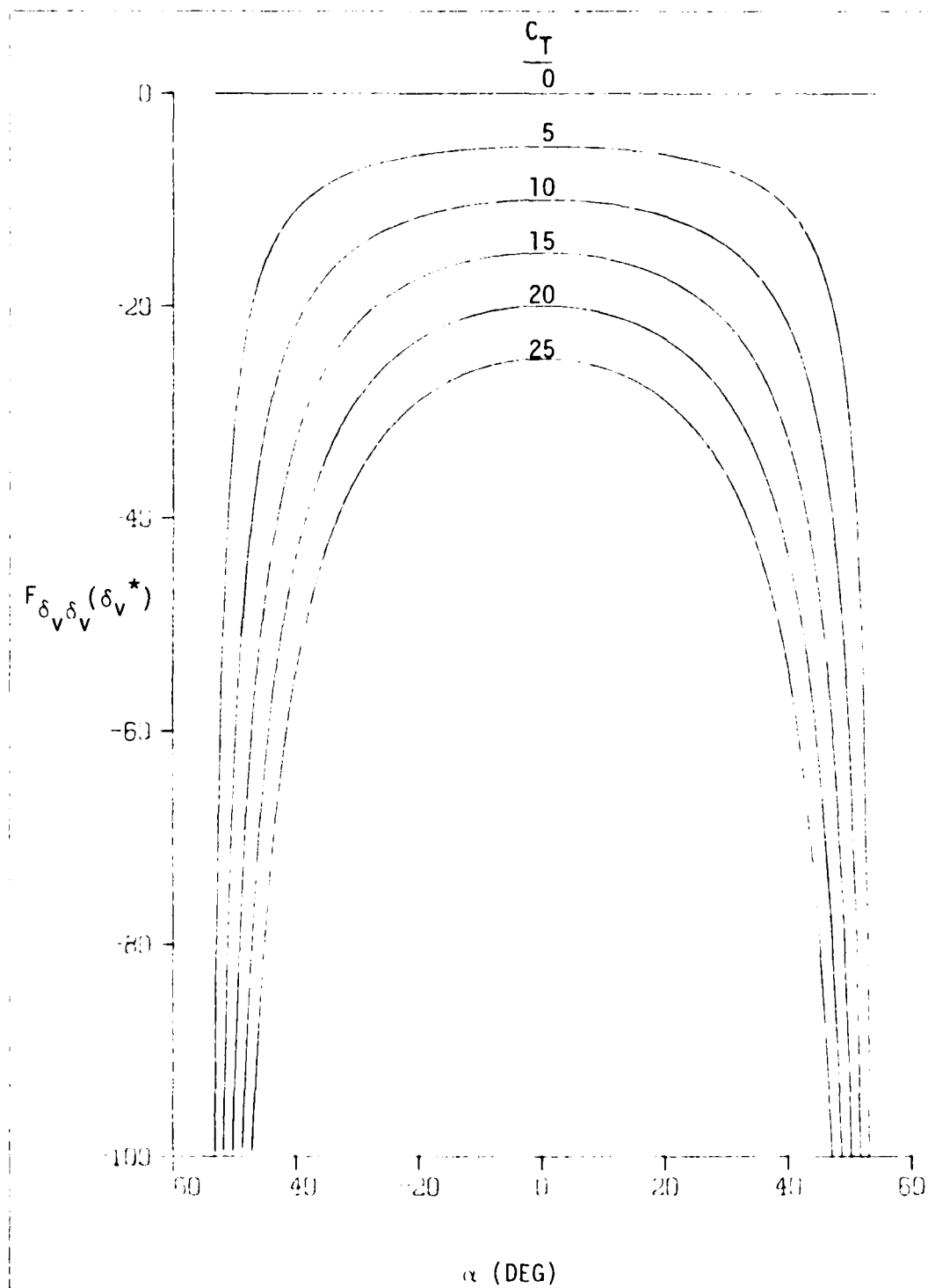


Figure 12. $F_{\delta_V \delta_V}(\delta_V^*)$

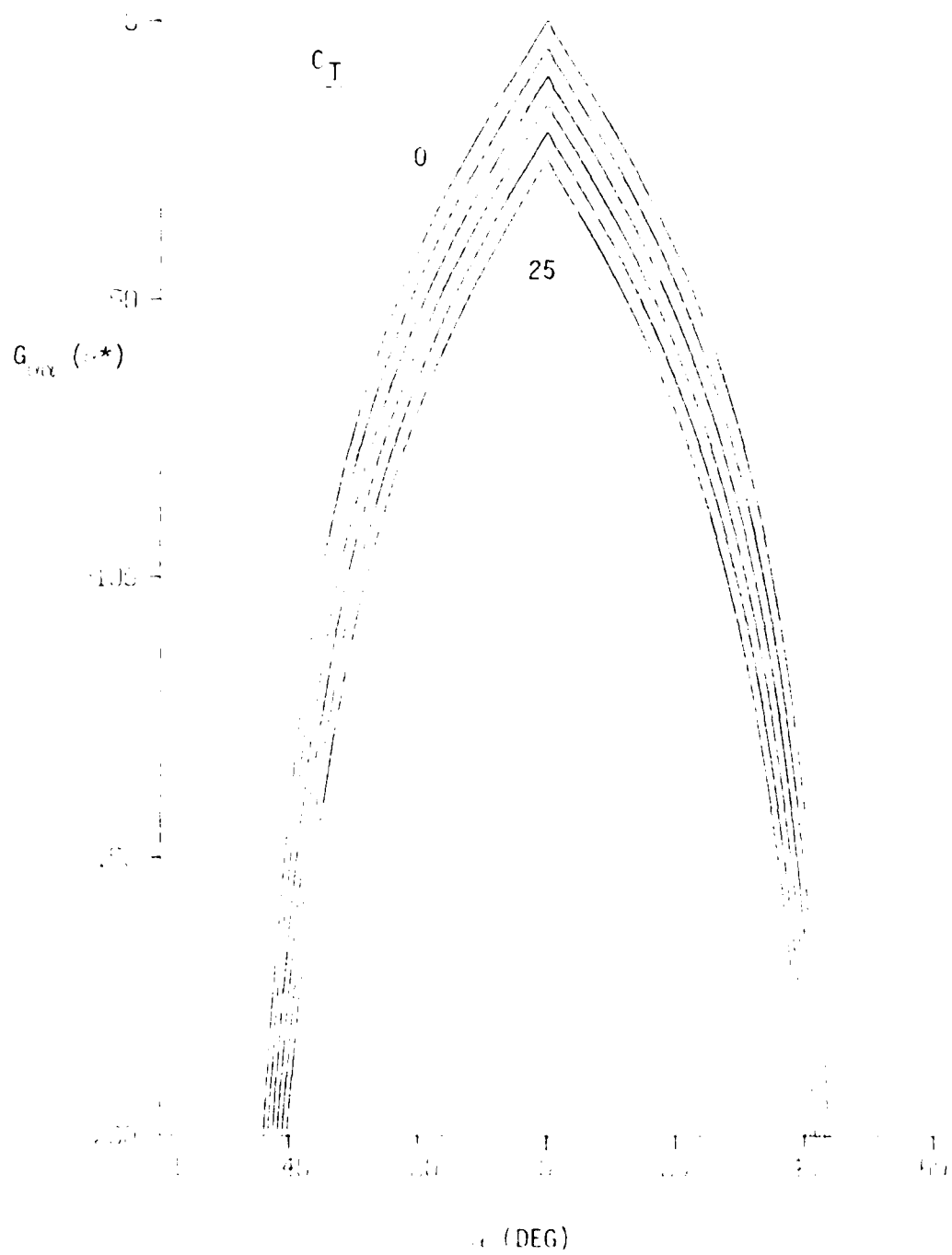


Figure 13. G_{max} (in $^\circ$)

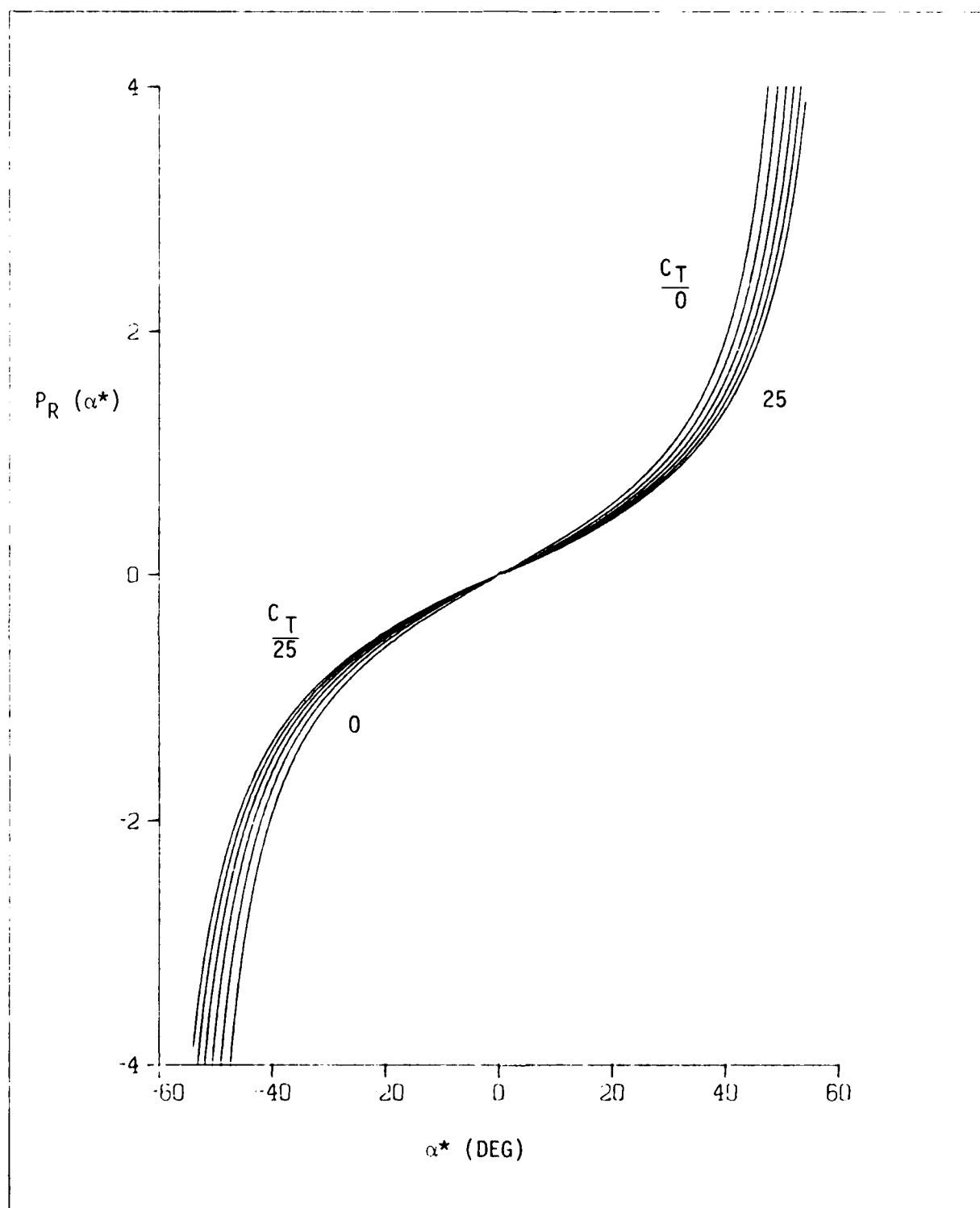


Figure 14. $P_R (\alpha^*)$, $\delta_V=0$

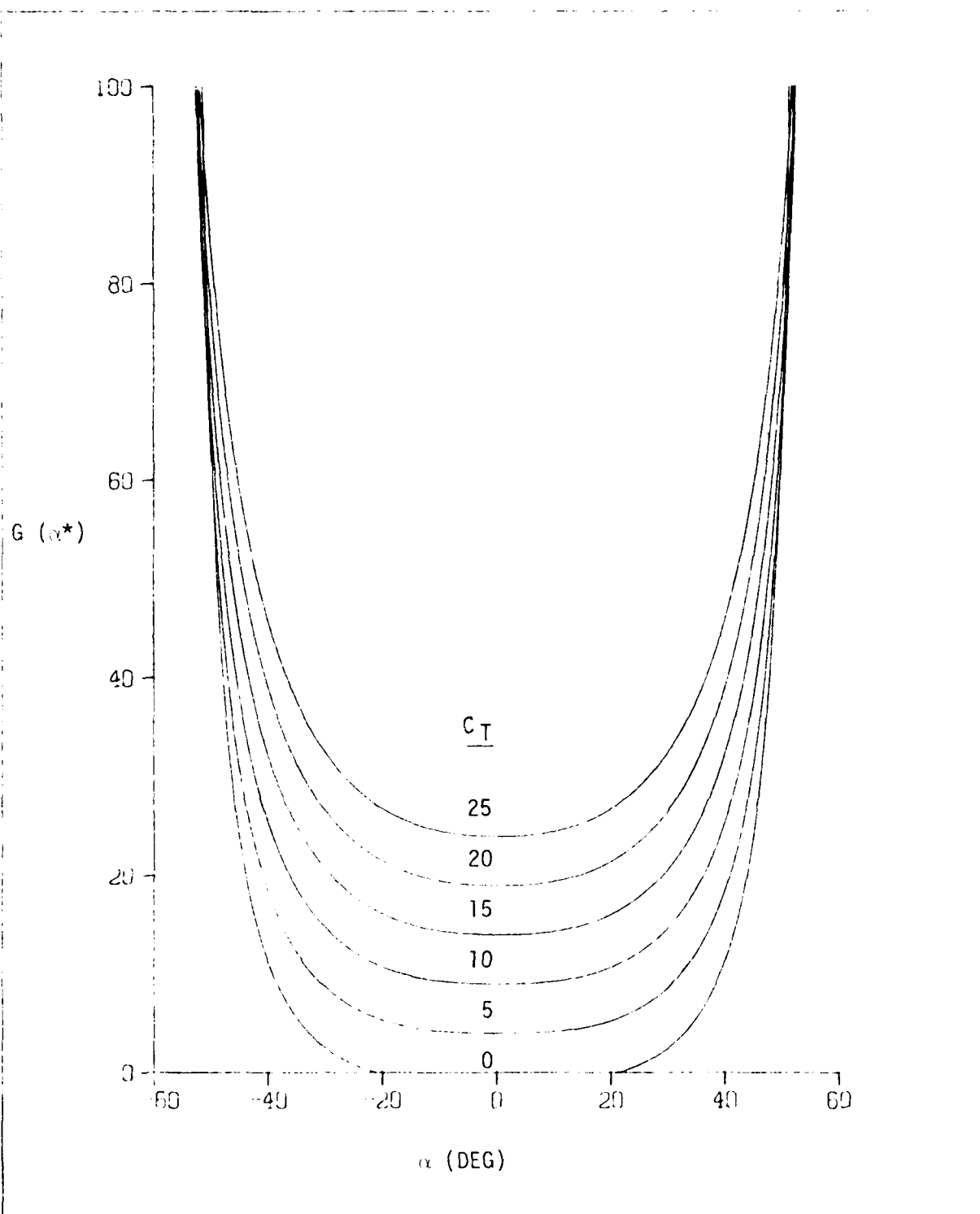


Figure 15. $G(\alpha^*)$, $\delta_V = 0$

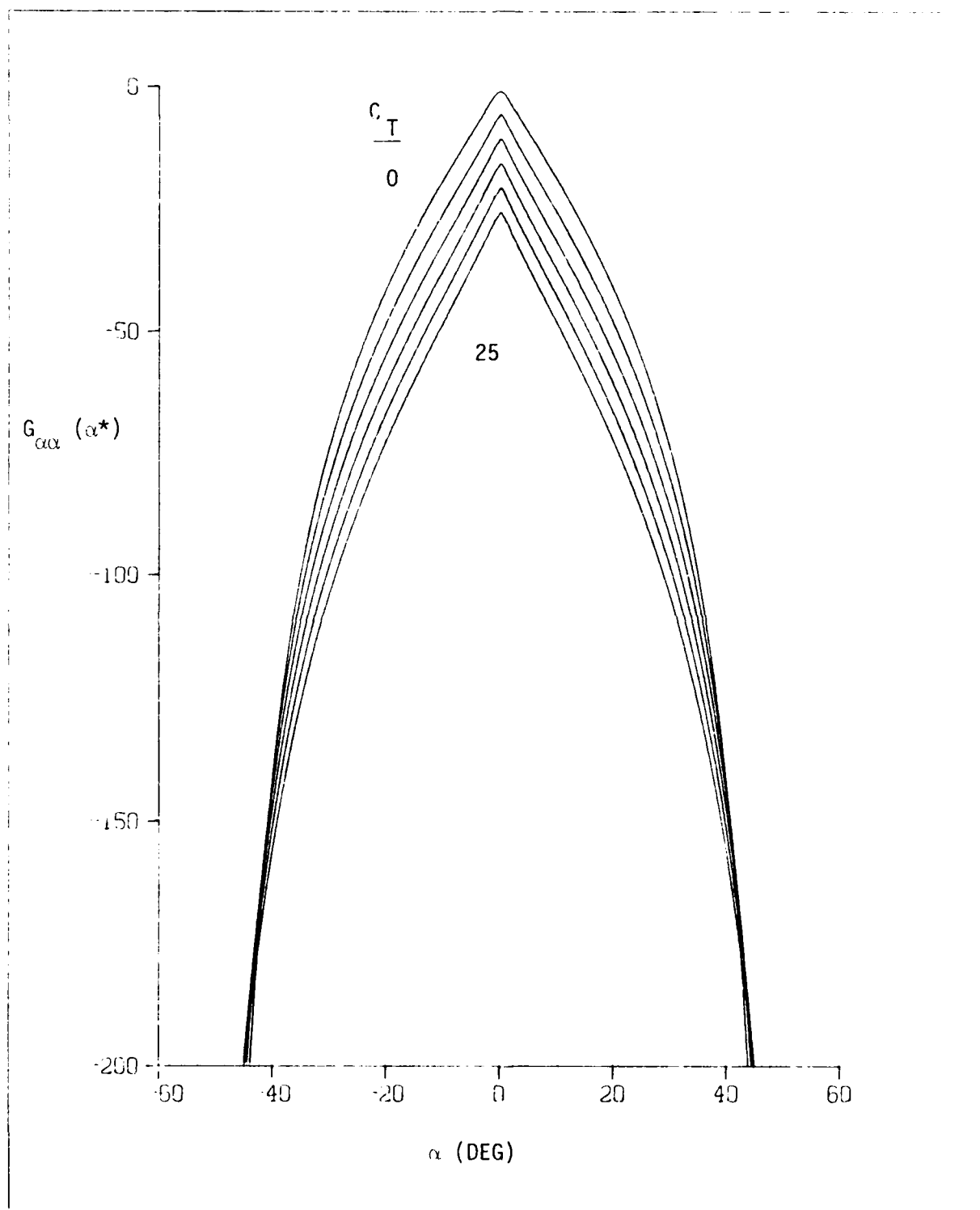


Figure 16. $G_{\alpha\alpha}(\alpha^*)$, $\delta_v = 0$

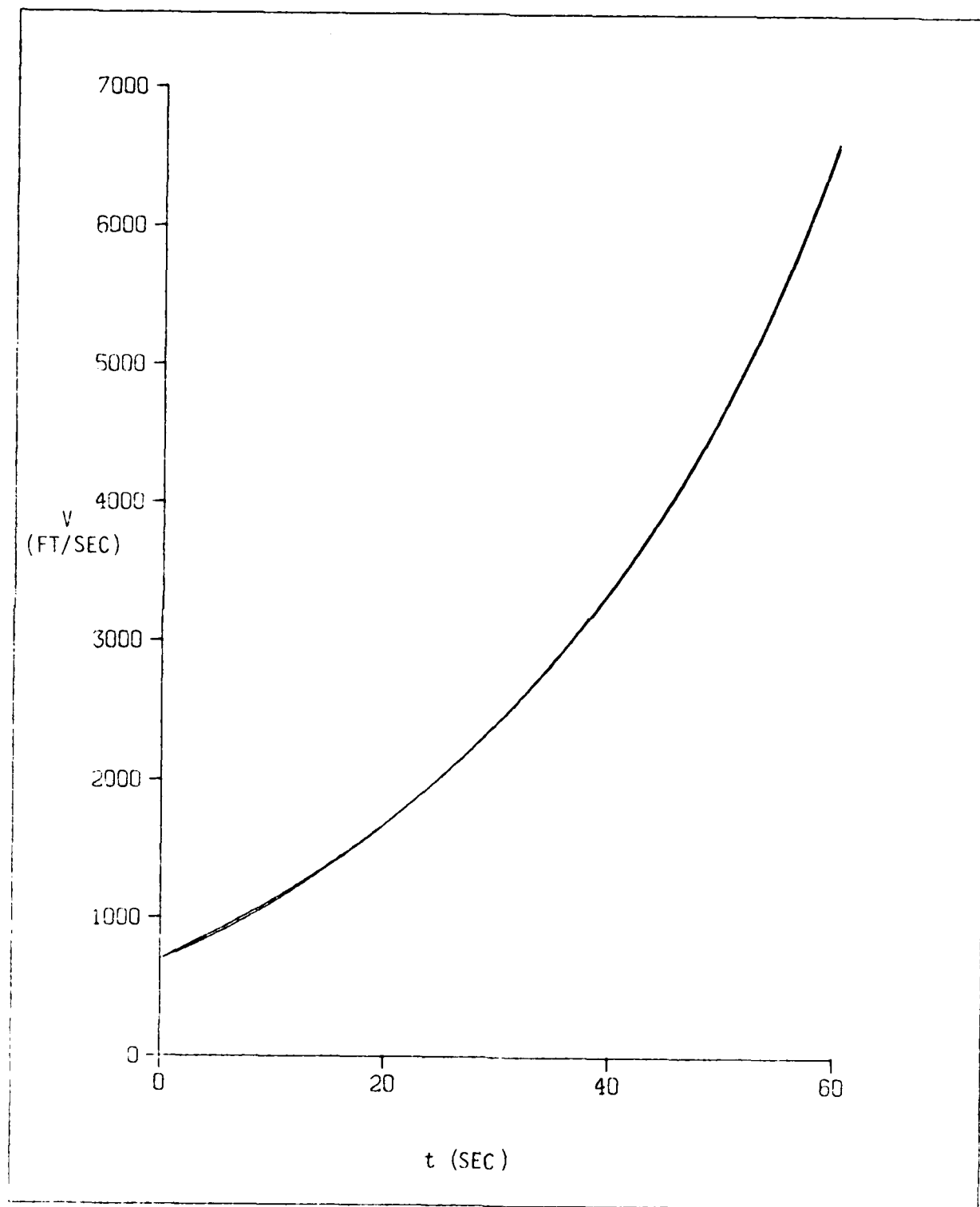


Figure 17. Optimal Speed, Problem 1

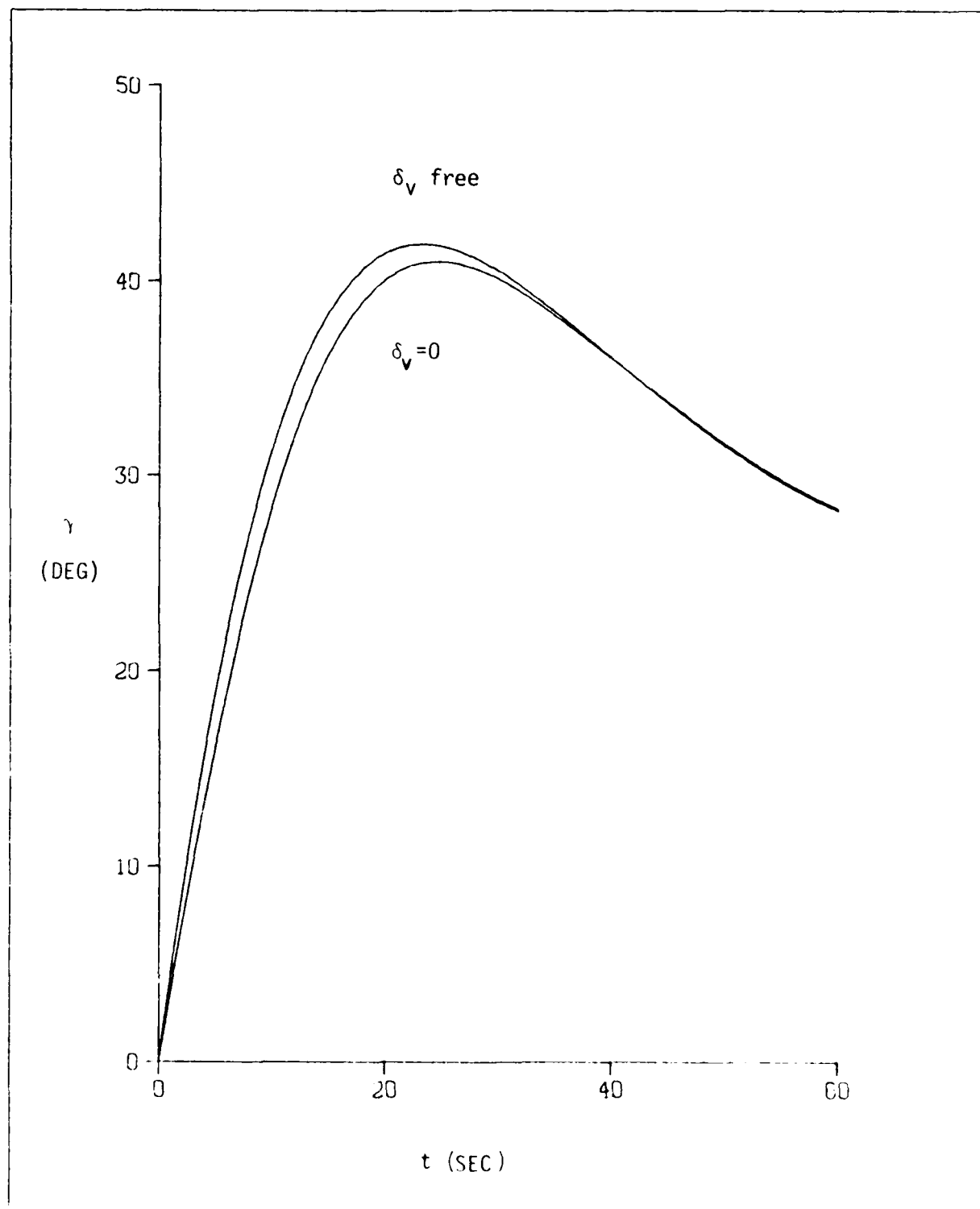


Figure 18. Flight Path Angle, Problem 1

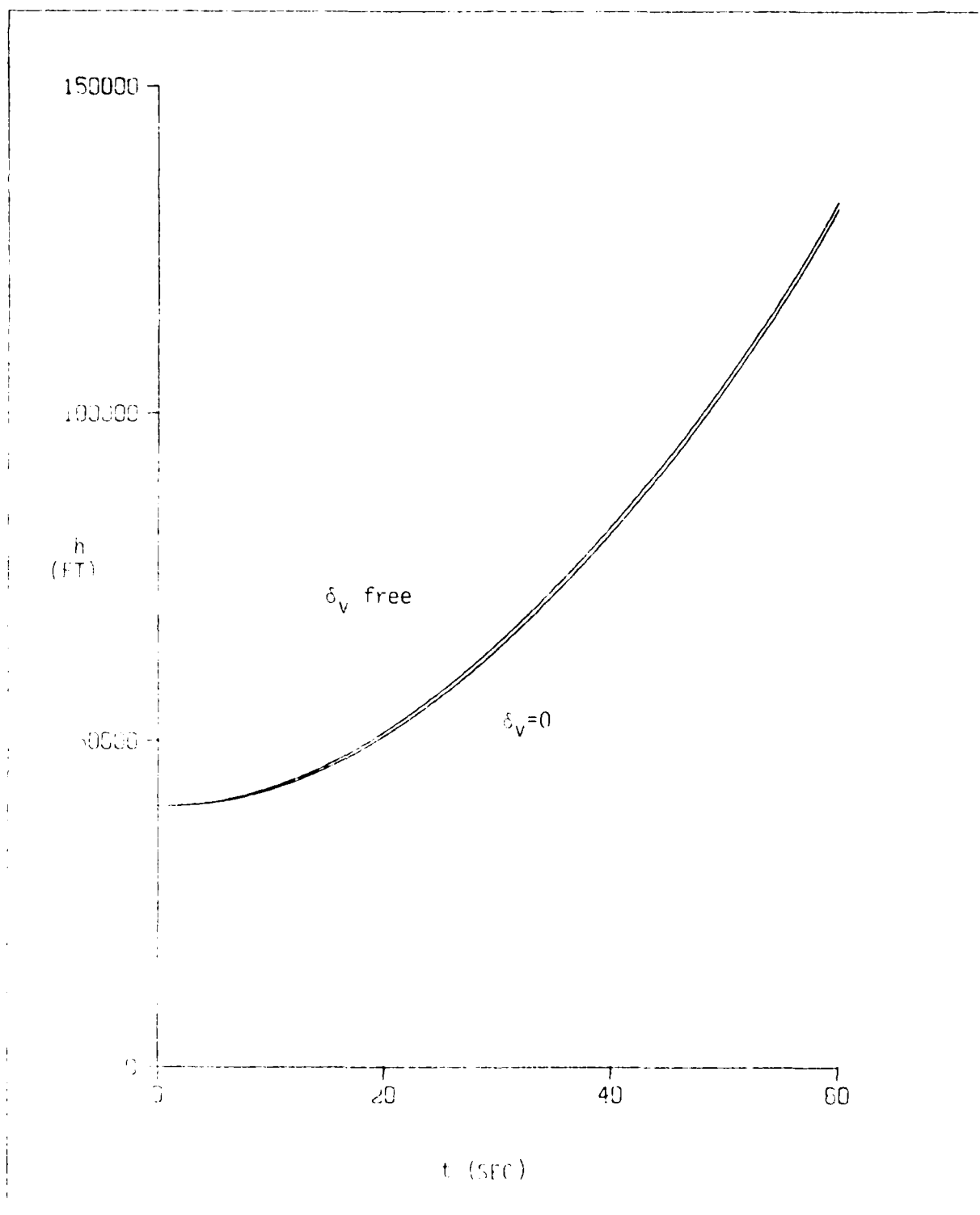


Figure 19. Altitude, Problem 1

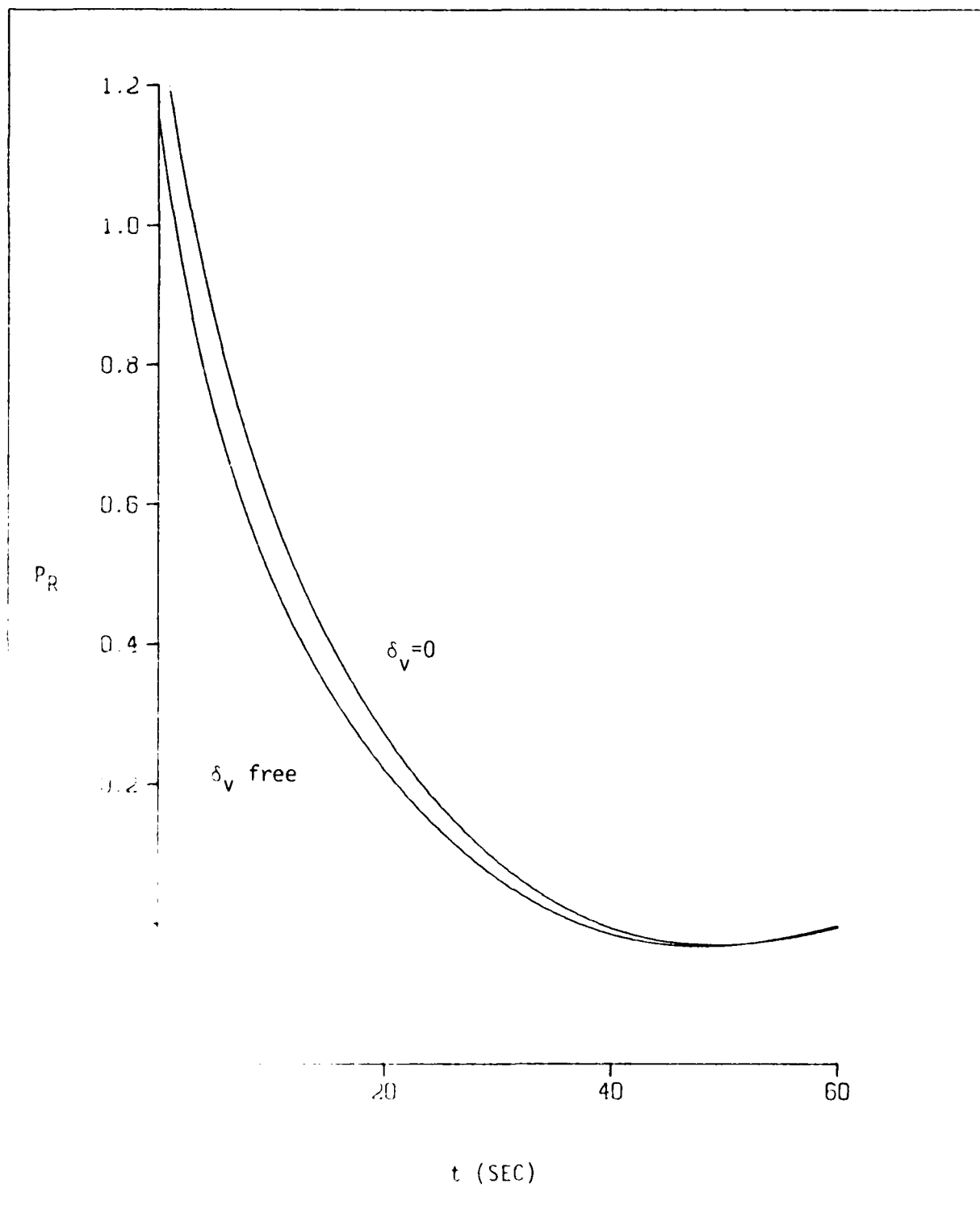


Figure 20. P_R , Problem 1

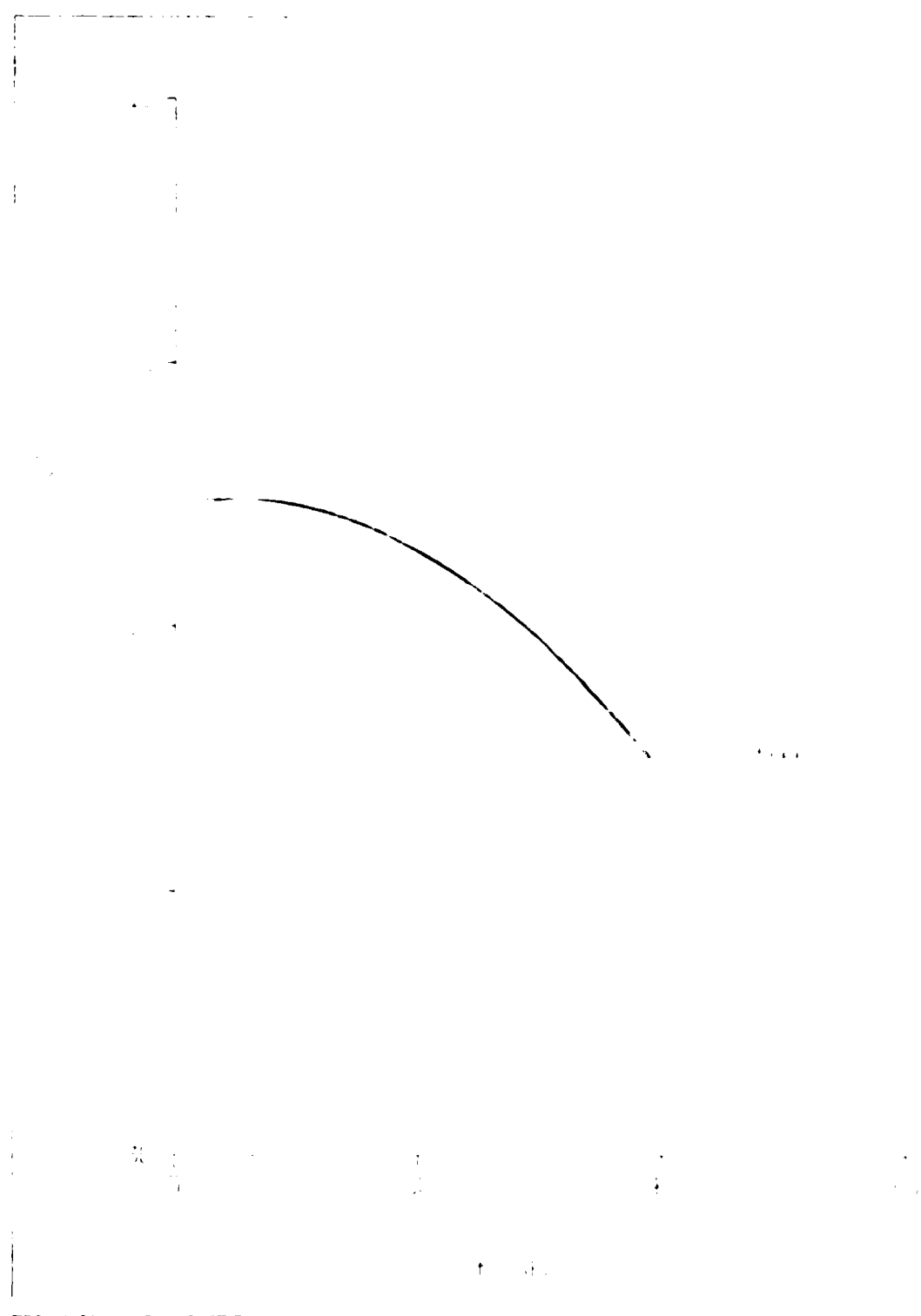


Figure 21 α , (b) plot 1

1. 1

2. 1

3. 1

4. 1

1. 1

1. 1

1. 1

1. 1

1. 1

1. 1

1. 1

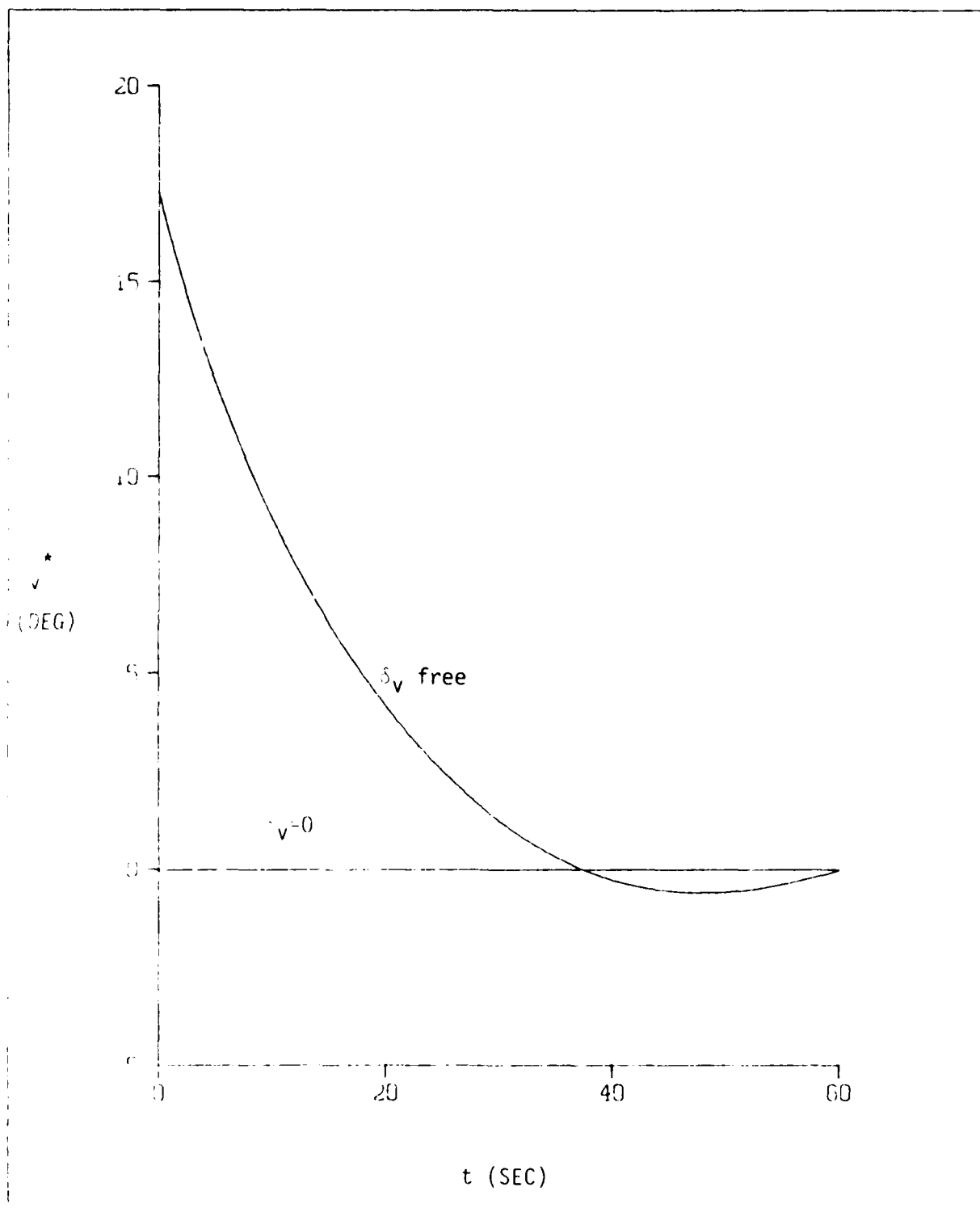


Figure 23. δ_v^* , Problem 1

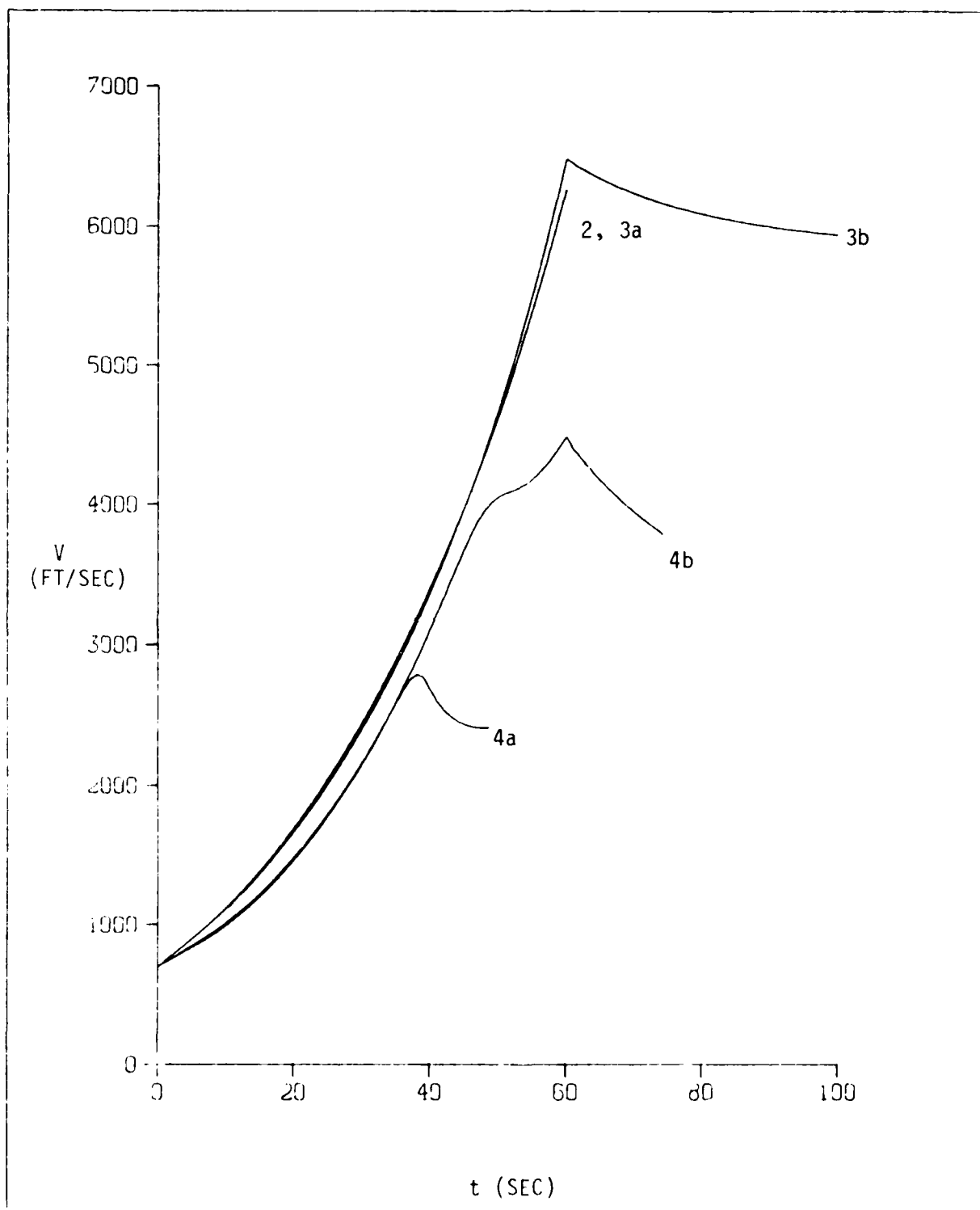


Figure 24. Speed for Problems 2, 3, 4.
 $\gamma(t_f)=0, \dot{\alpha}_V=0$

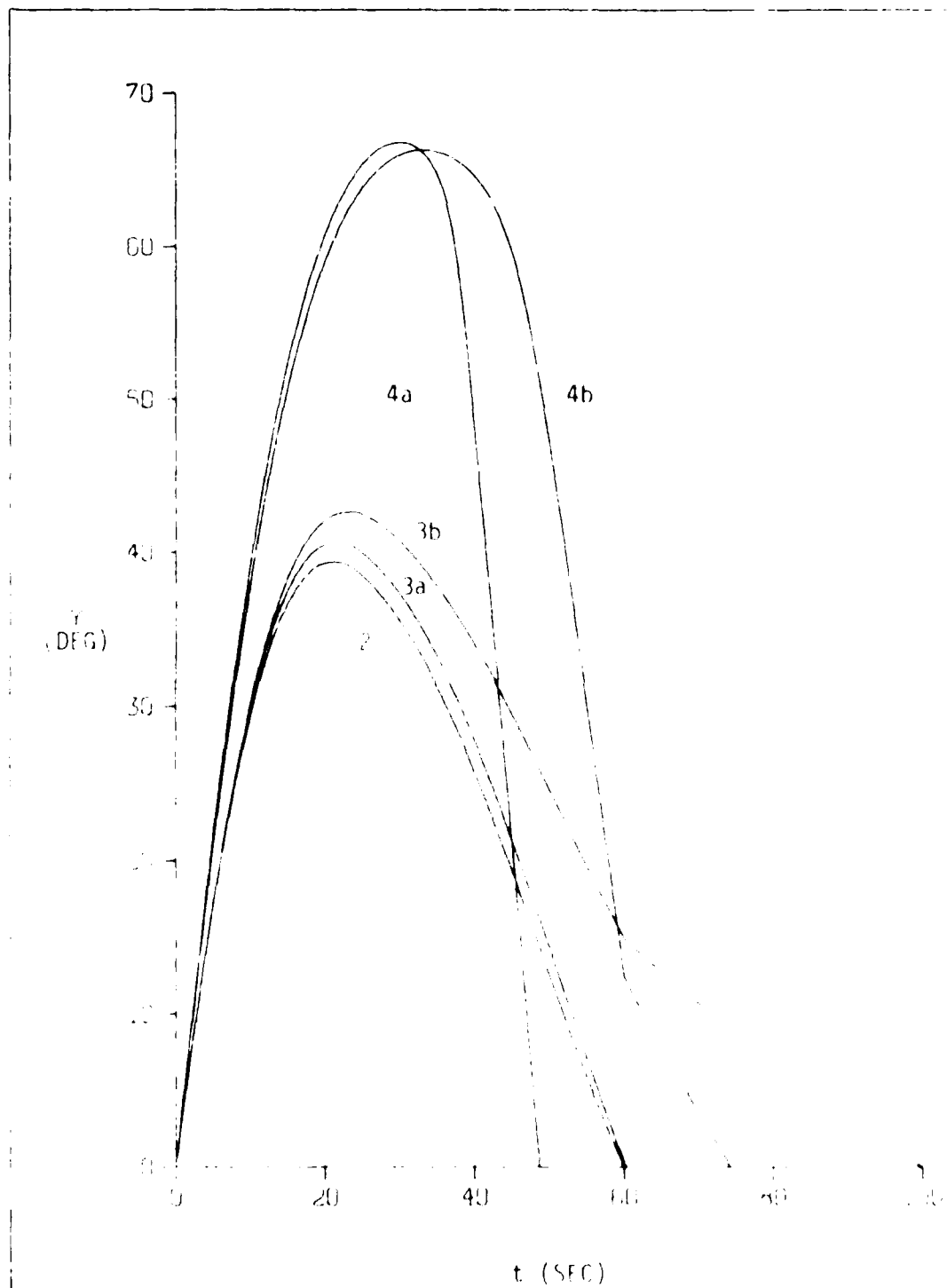


Figure 25. Flight Path Angle for Problems 2, 3, 4.
 $\gamma(t_f)=0, \dot{\gamma}_V=0$

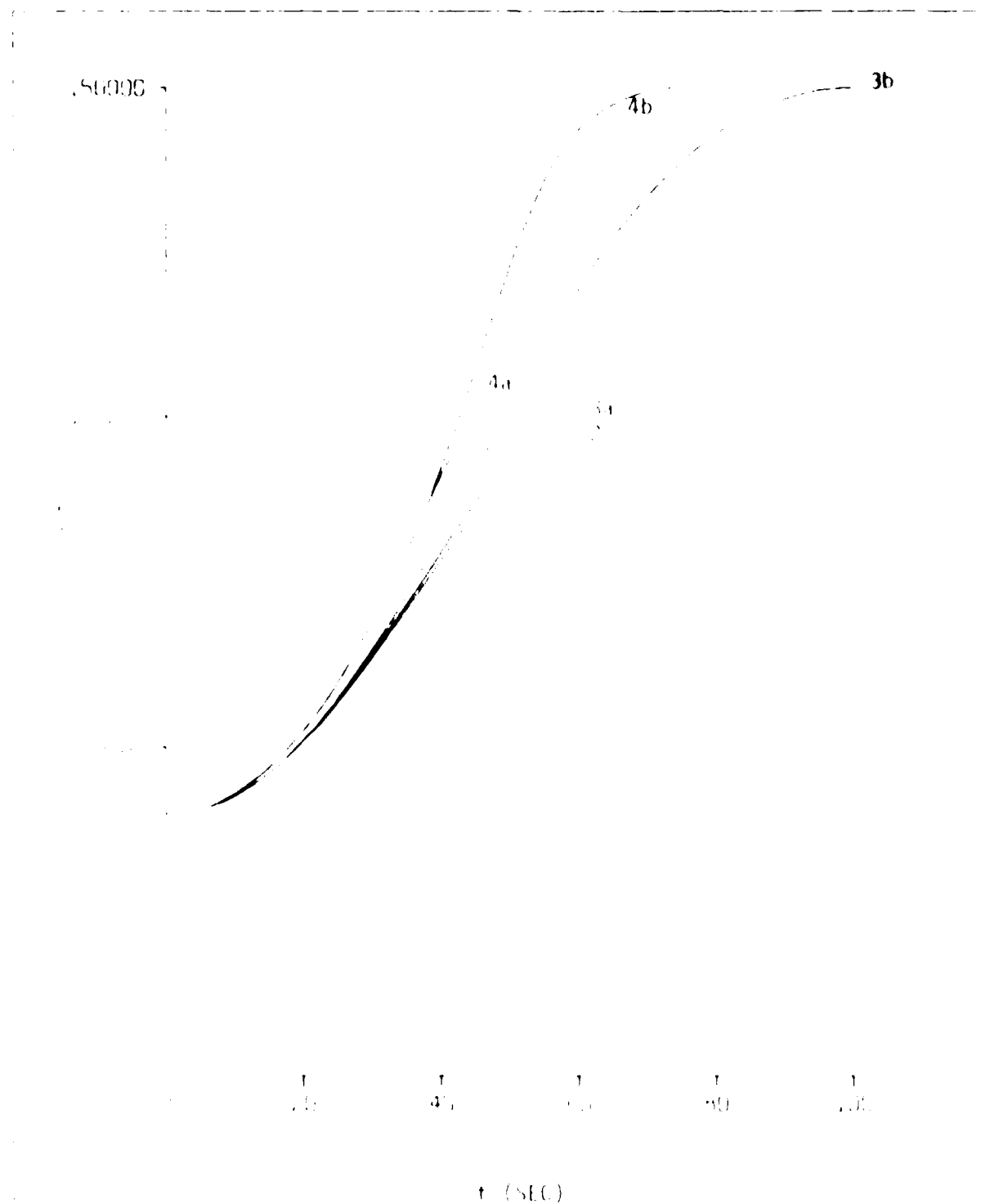


Figure 26. Altitude for Problems 2, 3, 4.

$$v(t_f) = 0, \quad v = 0$$

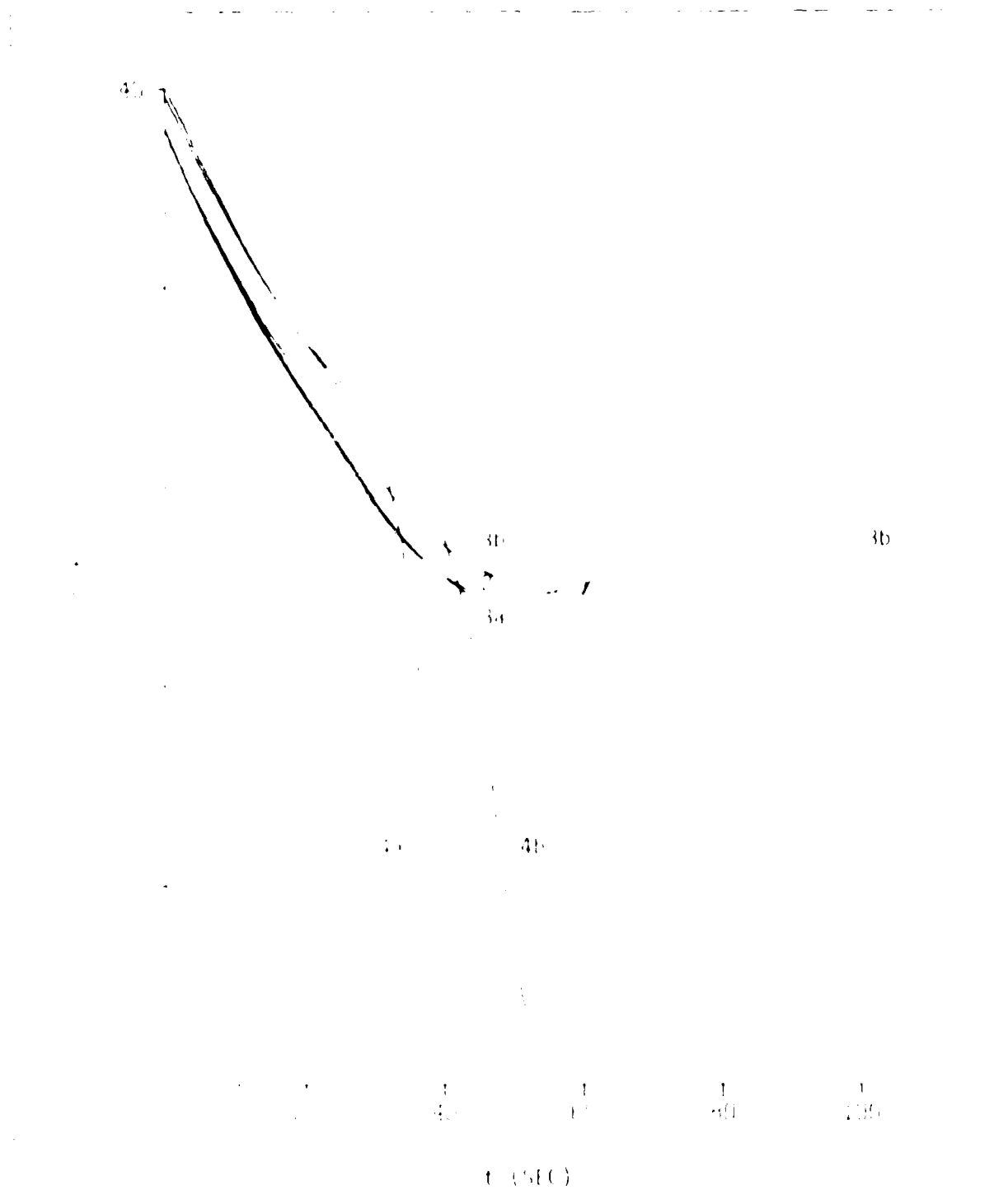


Figure 27. Optimal Angle of Attack for Problems 2, 3, 4.

$$v(t_f) = 0, \quad v = 0$$

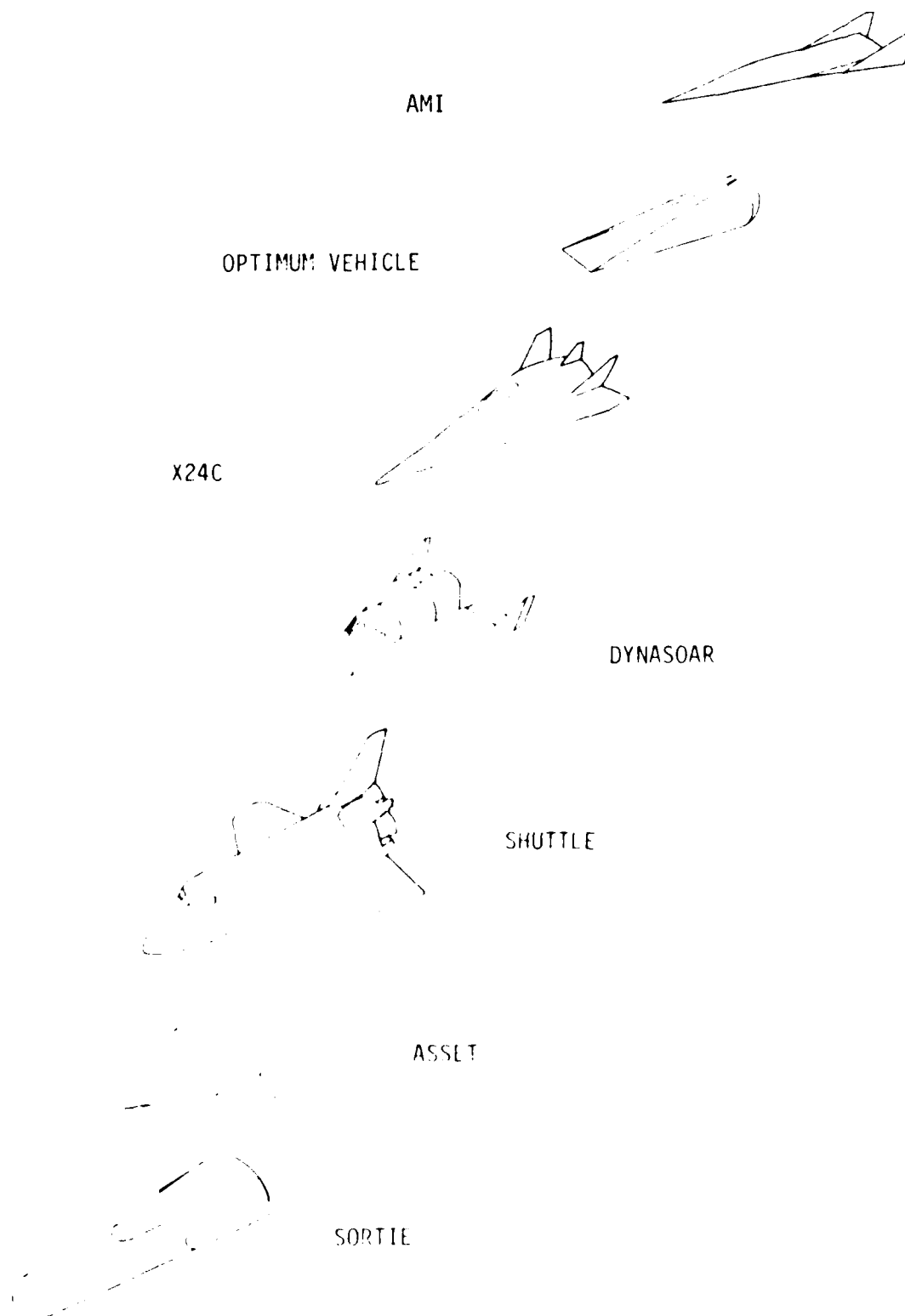


Figure A.1. Configurations

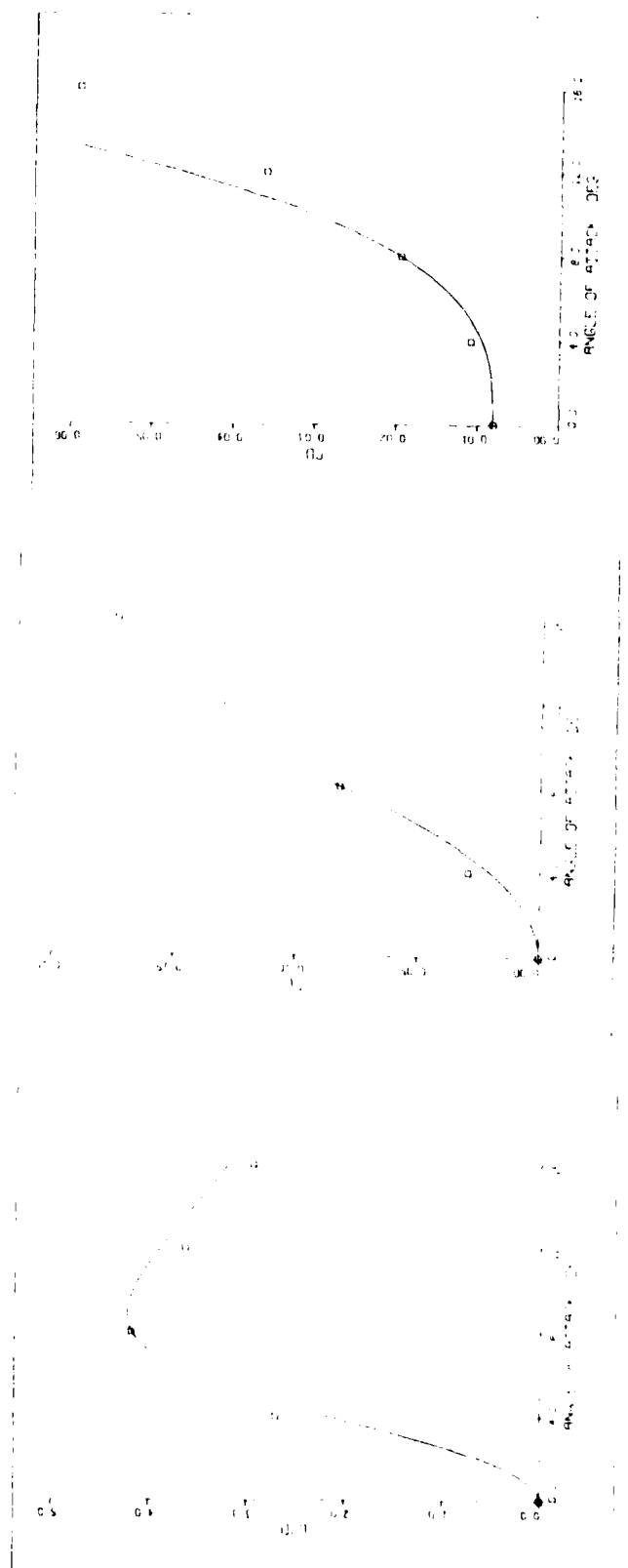


Figure A.2. AMI Aerodynamic Characteristics

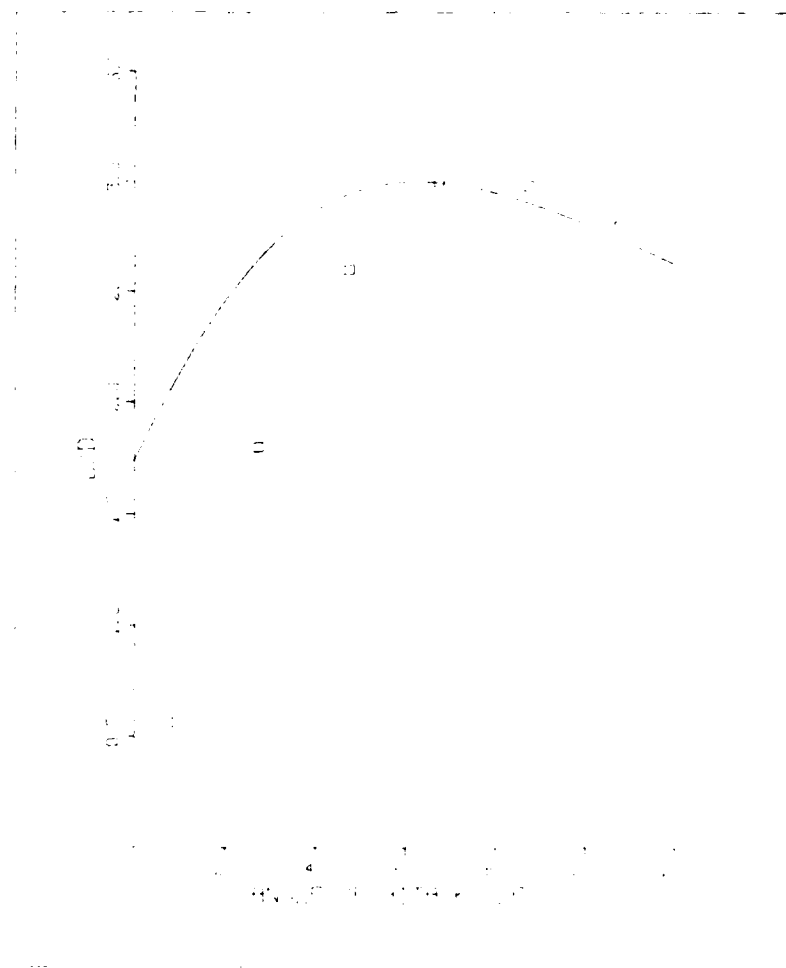


Figure A.3. Lift to Drag Ratio for Optimum Configuration

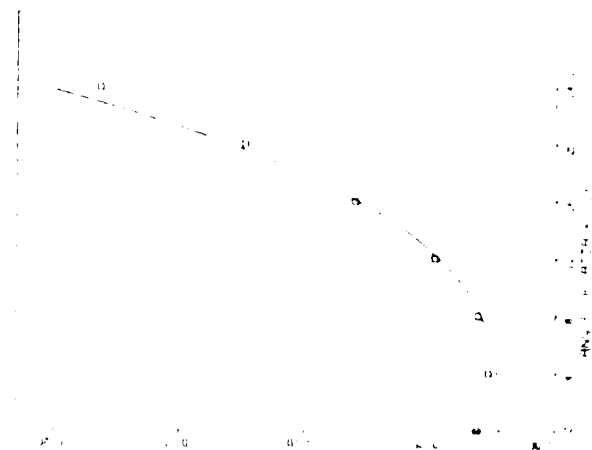


Figure A.4. X24C Aerodynamic Characteristics

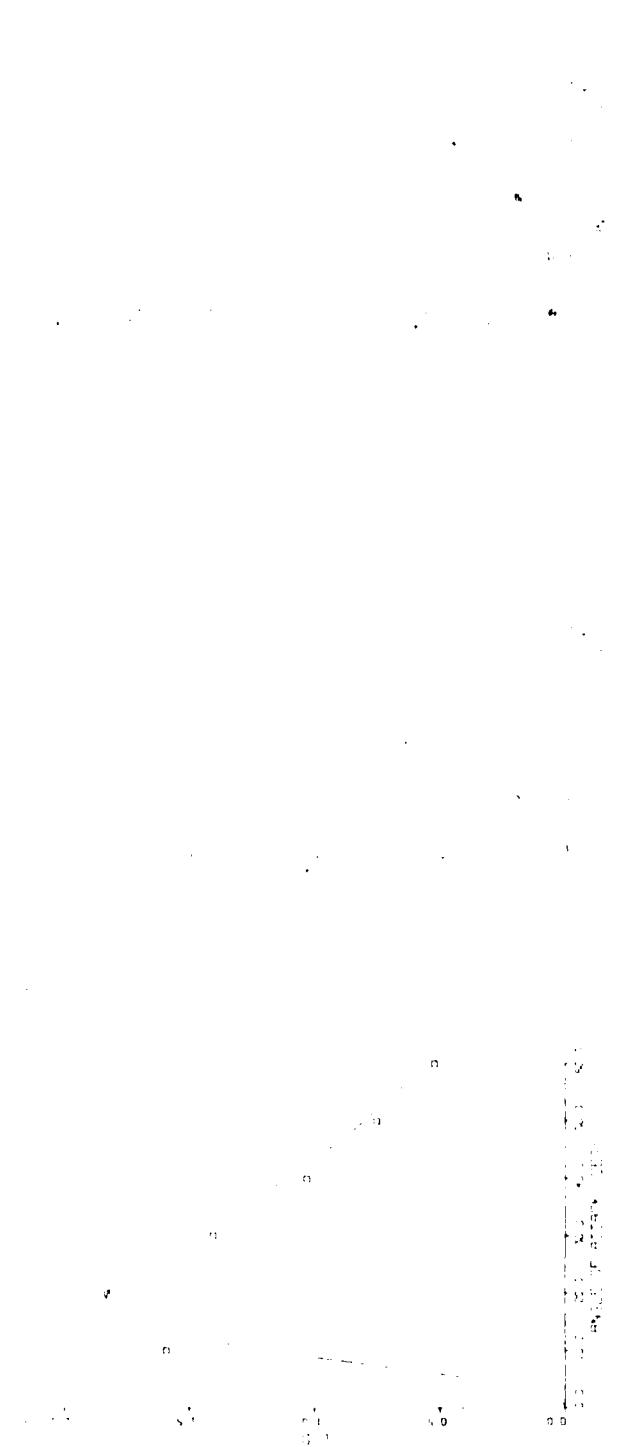


Figure A.5. DYNASOAR Aerodynamic Characteristics

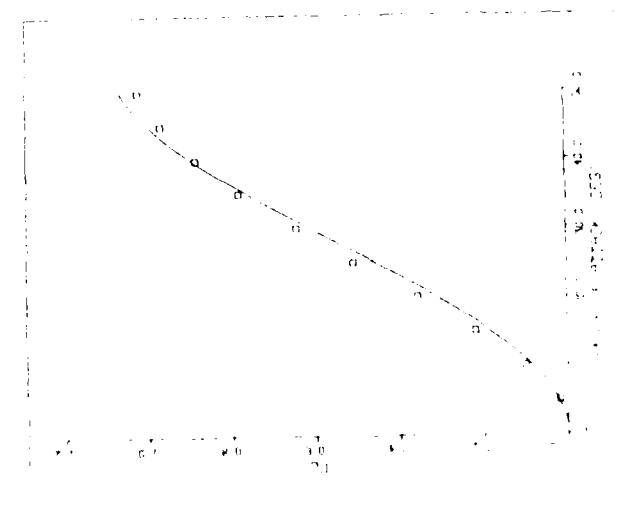
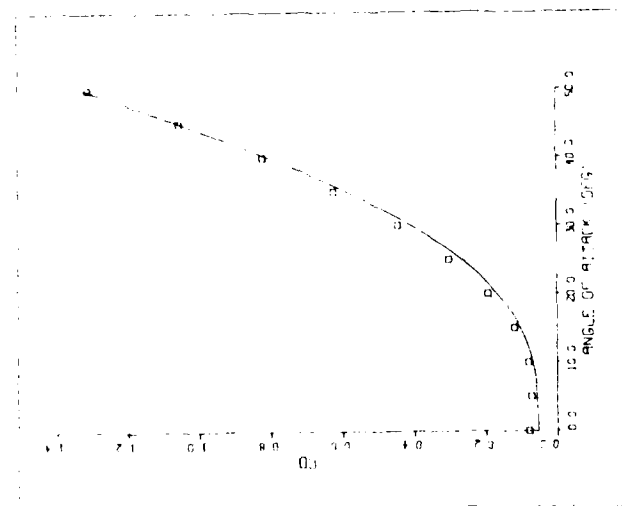


Figure 2.6. SHUTTLE Aerodynamic Characteristics

AD-A177 639

HIGH-SPEED PERFORMANCE ANALYSIS NOMINAL AND OPTIMAL
BOOST CLIMB PERFORMANCE (U) AIR FORCE WRIGHT
AERONAUTICAL LABS WRIGHT-PATTERSON AFB OH L E MILLER
JAN 87 AFMIL-TR-86-3875 F/G 28/4

2/2

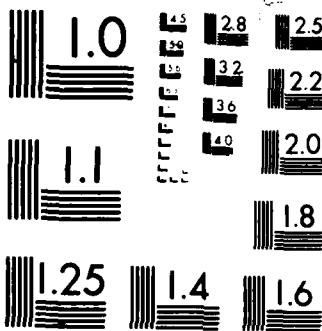
UNCLASSIFIED

ML

IND

q 8/

DIR



PHOTOCOPY RESOLUTION TEST CHART

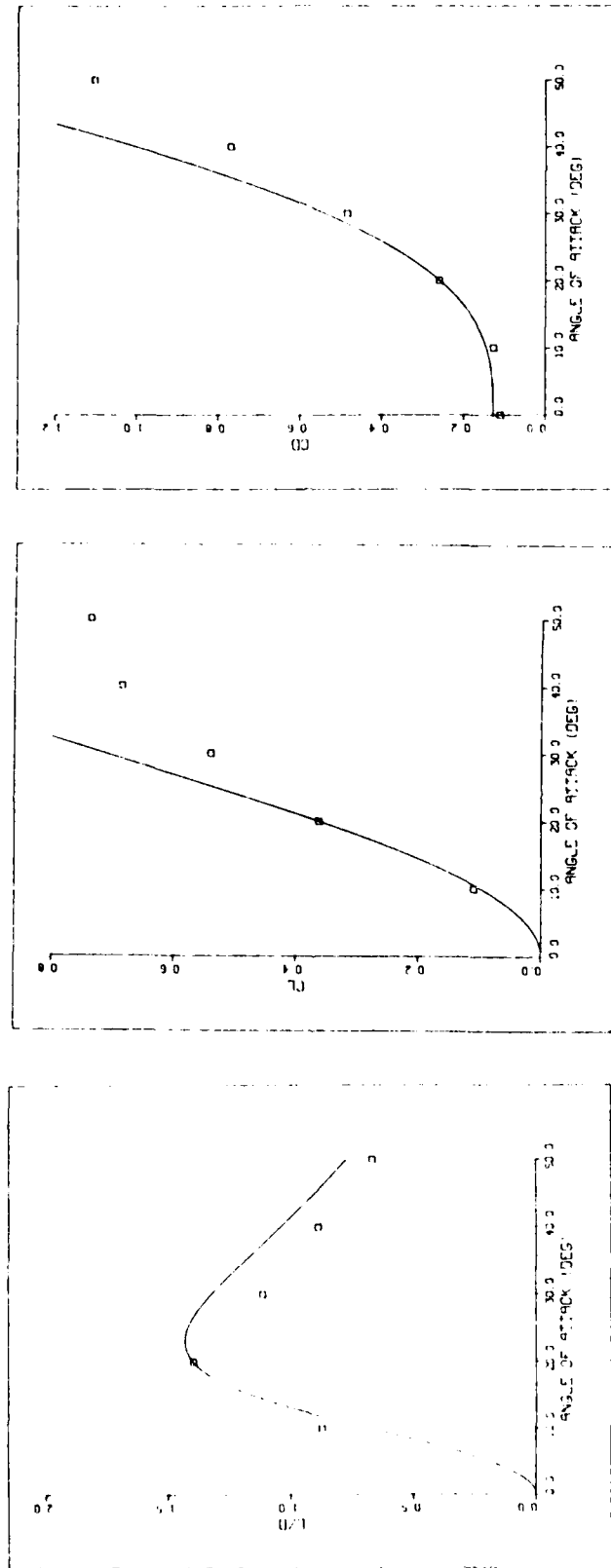


Figure A.7. ASSET Aerodynamic Characteristics

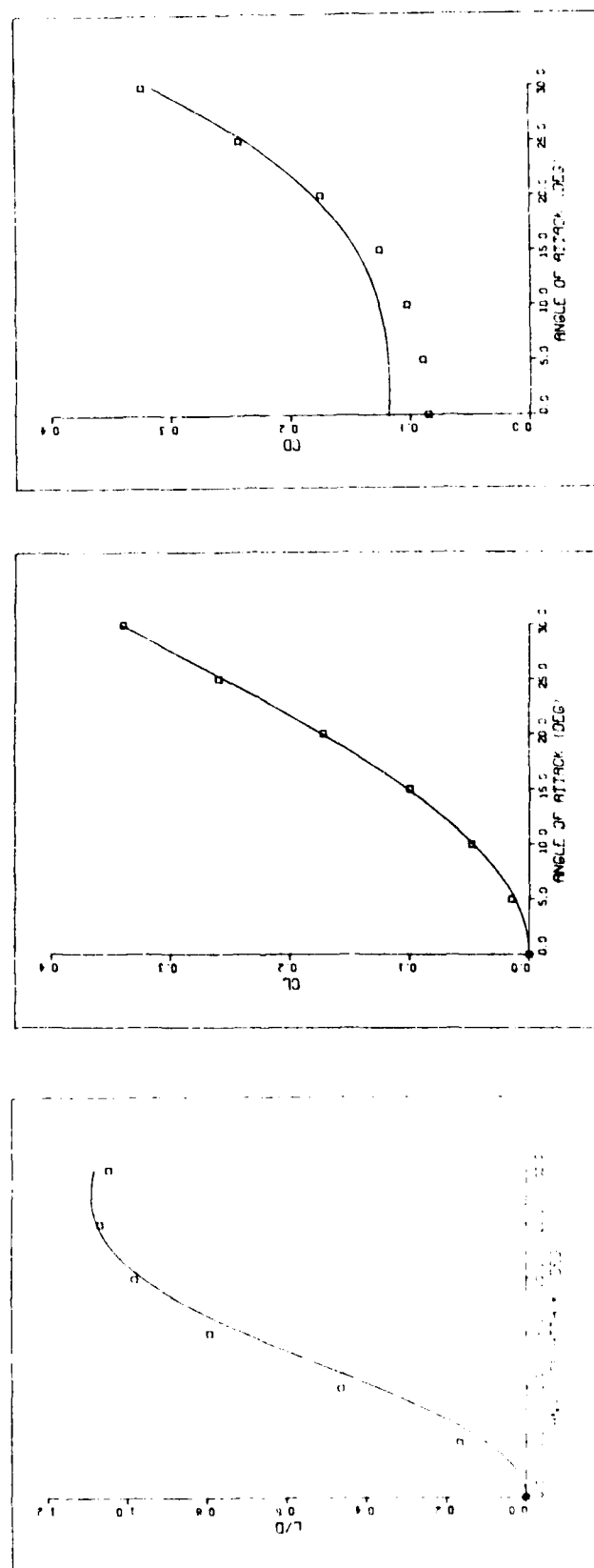


Figure A.8. SORTIE Aerodynamic Characteristics

END

4-87

DTIC